Biochip-Integrable Microfluidic Particle Separation Techniques for Biomedical Use

Biochip-Integrable Microfluidic Particle Separation Techniques for Biomedical Use

András József Laki

Department of Electronics and Telecommunications
Polytechnic University of Turin

Supervisors:
Kristóf Iván, Ph.D.
Pierluigi Civera, Ph.D. †
Danilo Demarchi, Ph.D.

A thesis submitted for the degree of
Doctor of Philosophy

January 2015

Acknowledgements

I would like to thank my advisors Kristóf Iván, Pierluigi Civera, and Danilo Demarchi for keeping me on track. You were always a source of new, and different perspectives to every problem. I greatly appreciate all of the help from the members of the Department of Genetics, Cell- and Immunobiology, the Department of Biophysics and Radiation Biology at Semmelweis University, and the Faculty of Veterinary Science at Szent István University especially Edit I. Buzás, Miklós Kellermayer, and Éva Fok.

I am grateful to Péter Fürjes and the MEMS Laboratory at Research Centre for Natural Sciences of Hungarian Academy of Sciences for helping me in the fabrication of our microfluidic devices.

I have been blessed with a wonderful family that has been an unending source of support and encouragement. I especially want to thank my parents for giving me strength to continue and hope to allow me to persevere. Finally, I give my deepest thanks to Ágnes for her amazing love and support.

Abstract

Biochip-integrable sorting and separation of micron-sized particles have an increasing importance in biomedical diagnostics, biochemical analyses, food and chemical processing, and environmental assessment. By employing the unique characteristics of microscale flow phenomena, various techniques have been established for fast and accurate separation, and to sort cells or particles in a continuous manner. As in classical separation procedures, the biochip-integrable size-fractionation of particles or cells could be realized by passive or active way. Passive procedures, which do not require external force-field, utilize the interaction between particles-particle, flow-particle, and the channel structure-particle to separate different-sized particles. Meanwhile, the active separation techniques make use of external force-field in various forms.

This doctoral thesis provides a novel biochip-integrable pathogen detection device (Flow Through Nematode Filter, FTNF), and a novel application of an asymmetric column structure, which called deterministic lateral displacement (DLD) device. The working principles are explained in detail, and performances of the devices are discussed with the results of the measurements.

The main target of this represented work is applications in medicine and biomedical research but we are also open for other application areas. The use of these simple microfluidic devices will make it possible to extend the use of cell-sorting to the point of care, closer to the patient at the clinic or in the field.

Keywords: Biochip-integrable fractionation procedures · Pathogen enrichment from blood · Blood fractionation · Microvesicle separation from serological samples

Contents

List of Abbreviations

γ	surface tension
μ	shear viscosity
μ_e	effective viscosity
ν	kinematic viscosity
$\vec{\mathbf{v}}$	velocity vector
ρ	density
ρ_p	density of particle
τ	viscous stress tensor
τ_f	characteristic time of the flow
τ_p	relaxation time of the particle
a_{grav}	gravitational acceleration
B	wetted perimeter
D	diffusion coefficient
D_H	hydraulic diameter
$d_{particle}$	diameter of the particle
F	body force
k_B	Boltzmann's constant
L	length of channel
P	pressure
Pe	Péclet number
$r_{particle}$	radius of the particle
r_{tube}	radius of the tube
Re	Reynolds number
Re_p	particle Reynolds number
St	Stokes number

Chapter 1

Introduction

Microfluidics concerns design, fabrication, and experiments of miniaturized fluidic systems, which has undergone rapid developments during the last decade [1]. As an interdisciplinary area, this rapidly growing field of technology has numerous applications in biomedical diagnostics, chemical analysis, automotive, and electronics industries [2]. One of the pivotal applications of microfluidics is the development of lab-on-a-chip (LOC) devices as point-of-care (POC) diagnostic tools. A typical LOC device includes various functional modules: sample transportation, sample preparation, separation, detection, and analysis module [3, 4]. The label-free size separation of particles or cells is vital to many of the analytical and preparative techniques used in the fields of chemical, biochemical, and clinical analysis, which led to ground breaking advances in terms of the speed of analyses, the resolution of separations, and the automation of procedures [5]. Additionally, microfluidic separator devices can form a part of portable systems for point-of-care or in-the-field detection [6].

Several variations of microfluidic cell sorters, which implement different sorting mechanisms, have been designed and fabricated [7, 8]. The chosen method of particle handling is generally based on the nature of the application, which strongly depends on the composition of the sample and the final goal of the analysis also should be under consideration. Several strategies exist for this purpose based on specific cell/particle characteristics including manipulation of particles in fluids or removal of particulate matter from fluids [9]. The particles may act or interact with the analyte, in which case they need to be removed from the sample [10].

1.1 Traditional Fractionation Techniques of Biological Suspensions

In traditional cell isolation processes, size separation is commonly used to separate mixtures of cells or particles before subsequent analysis or culture [10]. Cells exhibit variations in their hydrodynamic radii stemming from changes in volume, shape or mechanical properties, dependent on their state of health [11]. The existing cell separation methodologies can be classified into two main groups to enrich selected subpopulations [8]. The first group is based on physical criteria like size, shape, and density differences and includes filtration and centrifugation techniques, which are commonly used for debulking heterogeneous samples [12, 13]. The second group comprises affinity methods such as capture on affinity solid matrix (beads, plates, fibers) [14–16], fluorescence-activated cell sorting (FACS) [17, 18] and magnetic cell sorting [19, 20], which are based upon biochemical cell surface characteristics and biophysical criteria [8].

Traditional fractionation instruments ranging in size from desktop to room sized models are standard pieces of equipment at most large hospitals and are used to analyse and separate cells and other biological particles [21]. Another drawbacks of the existing, traditional flow cytometers are that these devices are expensive, require an extensive infrastructure such as facilities, personnel and reagents, does not suited to integration with other analysis steps, and time is needed to process the signal data limits the rate at which cells can be detected. Much work is therefore being done to develop methods that will not only be cheaper, and therefore more easily available, but also more effective and possibly able to probe particle properties not currently accessible [21].

In clinical diagnostic sense, cell sorting and counting devices are examples of technological solutions that have been designed and optimized for use in centralized laboratories, much like the very first computers. Also nowadays the biological samples (blood, urine, other biological liquids) are collected from patients at the hospitals, at home or in special environments and sent to these centralised diagnostic laboratories where analysis takes place. However the transportation of samples also takes money and time, and the quality of samples be decayed or modified due to the natural biological reactions.

1.2 Novel Separation Technologies Integrated into Biochips

The trend in life science research to miniaturize analytical processes using biochips, first proposed in the late eighties, is ongoing [1]. The benefits of miniaturization and integration are many including increased automation, parallelization, speed, resolution and portability as described in reviews by Mosadegh [22], Craighead [23], Mark [24], Erickson [25], Franke [26] and Dittrich [27]. The idea of integrating sampling, sample handling, reactions, separations and detection into one automated device containing interconnected microchannel networks led to the introduction in the literature of the term micro-total-analysis-system (μTAS) in 1990 by Manz et al. who was performed first on-chip separation implementing capillary electrophoresis fractionation of fluorescent molecules [28, 29]. Since that time, applications of μTAS has developed over the past two decades exponentially, meanwhile scientific journals, conferences, and companies specializing in LOC technologies are evidence of how interest in this field has grown.

In sense of cell isolation, the efficiency of fractionation takes into consideration the available sample volume for analysis, the characteristic/feature that distinguishes the cell types, the required purity of the separated population with desired characteristics, the total number of cells lost during the process of separation, the viability of cells after separation and the physical stress endured by the cells. Finally, choosing an efficient sample handling procedure, the taken time for the complete cell separation process and the cost-effectiveness of the technique are also not negligible.

The integration of particle separation techniques into lab-on-a-chip devices is advantageous, as described by Pamme [30], that these label-free processes are continuous, the separation can be monitored continuously and the sample components are displaced laterally thus each fraction could be collected independently. Based on the applied forces the fractionation could be tangential or perpendicular to the flow direction and can be realised as batch or continuous loading procedures (Fig. 1.1). In batch separation techniques, the particles particles follow the same paths but at different rates which appears fractionation in time only thus these procedures requires precise injection of a very small amount of sample into the separation channel. At the other case, the applied forces have perpendicular components to the flow direction thus the particles are displaced laterally and become separated in space.

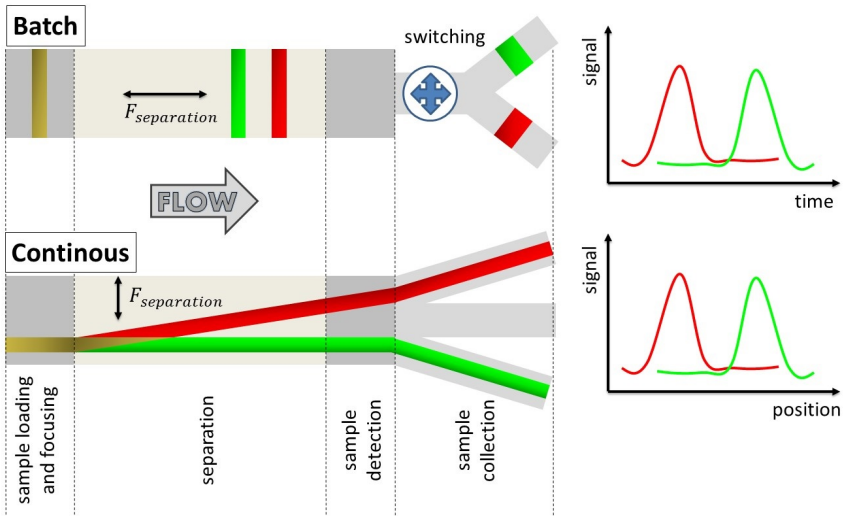

Figure 1.1: Batch separation procedure entails the injection of finite volumes parallel with the flow direction into a separation column. The separated sample fractions pass through a detector at different times, often followed by repeats to optimise separation parameters. Collection of the separated fractions can only be achieved with a flow switching mechanism that redirects different components to different outlets. Continuous procedure separate perpendicularly to the flow direction. The sample is injected continuously together with a carrier liquid, meanwhile the separation efficiency can be monitored in real-time. (adapted from Ref. [30])

A range of field flow fractionation (FFF) techniques have been reported for separation of particles in lab-on-a-chip based microfluidic systems [30] since FFF method was pioneered by Giddings in 1960s [31]. The continuous-loaded single-phase field flow fractionation requires external forces or uses only inertial shear forces.

Large variety of methods have been developed to date that operate by external forces but in each case, the special cell properties and attributes have to be taken into consideration. Table 1.1 gives an overview of the different continuous particle separation methods which are based on external perpendicular forces to the direction of flow and focuses on the utilised external forces and the basis of separation. These separation methods can be classified by the applied external forces into acoustophoresis, dielectrophoresis, magnetophoresis, usage of mechanical forces and optophoresis.

The requirement of external forces increases the complexity of the device and may limit the application for some specific reagents such as biological samples. Consequently, researchers have been paying attention to the development of novel physical

Method	Separation induced by	Separation based on	References
Acoustophoresis	Acoustic pressure	Size, density, compressibility	[32–37]
Dielectrophoresis	Inhomogeneous electric field	Size, polarisability	[38–45]
Magnetophoresis	Inhomogeneous magnetic field	Size, magnetisation	[46–51]
Mechanical forces	Gravity, centrifugation	Size, density	[52–55]
Optophoresis	Optical force	Size, refractive index	[56–58]

Table 1.1: Listing of continuous flow separation methods using external forces with details of the forces utilised and the basis of separation were taken from the selected references.

methods (Table 1.2), which based on varying only the geometry of microchannels modifying the flow profile and influencing the local flow properties such as bifurcation channels, deterministic cell rolling (DCR), deterministic lateral displacement (DLD), pinched-flow fraction (PFF) devices, or applying Dean effect or using flow-through filters/membranes.

Hydrophoretic techniques	Separation based on	References
Bifurcation channels	Zweifack-Fung effect	[59–67]
Dean flow	Dean effect	[68–76]
Deterministic cell rolling (DCR)	Shear-induced and wall-induced lift	[77–82]
Deterministic lateral displacement (DLD)	Shear-induced and wall-induced lift	[83–101]
Flow-through filters (FTF)	Pressure field gradient	[102–108]
Pinched flow fractionation (PFF)	Shear-induced and wall-induced lift	[109–124]

Table 1.2: Listing of continuous flow separation methods using inertial forces with details of the basis of separation were taken from the selected references.

Comparison of performance of integrable sample fractionation methods is not always straightforward. Plenty of approaches offer high throughput, meanwhile others offer high resolution. Several of the microfluidic devices are simple in terms of operation, whilst other techniques might require a specialist. A number of separation principles

require labelling of sample components, whereas some processes are based on intrinsic sample properties. As always, the optimum method will depend on the sample and the analytical task at hand.

1.3 Scope of the Thesis

Chapter 2 discusses the main physical property of serological samples, which gives a brave discussion of hemodynamic principles is beyond the scope of this thesis but in this chapter, an overview of basic principles is presented that are helpful in understanding the physical background.

Chapter 3 discusses a novel biochip to observe uncovered parasitosis from serological samples. This chapter is based on work published in Springer - BioNanoScience [125] and presented in international conferences, which starts with a brave introduction, represents the physical principles, and shows the results of computational fluid dynamic simulations, and the experimental tests.

Chapter 4 discusses a novel application of the deterministic lateral displacement device. This chapter starts with the description of the physical principles, continues with computational fluid dynamics results and concludes with the representation of the experimental results using our own developed DLD structure to separate microvesicles from serological samples. The material presented in Chapter 4 excluding the discussion on the description of principles was also published in Springer - BioNanoScience [126].

Chapter 2

Hematology, Hemorheology, and Hemodynamics

2.1 Hematology

Blood (*sanguis*), perhaps the most important biological fluid, performs many fundamental functions to maintain homeostasis; from transporting nutrients and oxygen to tissues and organs to regulating pH and temperature. It also provides an efficient transit system through the vascular network for transport of immune cells for defense against foreign microbes and wound healing. As blood contains a myriad of information about the functioning of the human body, complete blood analysis has been a primary diagnostic test in our healthcare system.

The total body fluid is distributed mainly between two compartments: the extracellular fluid and the intracellular fluid. The extracellular fluid is divided into the interstitial fluid and the blood plasma. In the average 70-kilogram adult human, the total body water is about 60 % of the body weight, or about 42 liters [127]. This percentage can change, depending on age, gender, and degree of obesity. About 28 of the 42 liters of fluid in the body are inside the 75 trillion cells and are collectively called the intracellular fluid, which is almost the 40 % of the the total body weight [127]. All the fluids outside the cells are collectively called the extracellular fluid. Together these fluids account for about 20 % of the body weight, which is about 14 liters [127]. The two largest compartments of the extracellular fluid are the interstitial fluid, which makes up more than three fourths of the extracellular fluid, and the plasma, which

makes up almost one fourth of the extracellular fluid, or about 3 liters.

Blood contains both extracellular fluid (the fluid in plasma) and intracellular fluid (the fluid in the red blood cells). The average blood volume of adults is about 7 % of body weight, or about 5 liters [127]. The composition of the blood are cells and plasma (Table 2.1), which mostly comprises water and contains glucose, proteins, hormones, mineral ions, gases. The cells of blood (Table 2.2) presents are red blood cells (called RBCs or *erythrocytes*) white blood cells (called WBCs or *leukocytes*) and platelets (PLT, *thrombocytes*).

Name	Mass concentration $[mg/dl]$	Name	Mass concentration $[mg/dl]$
Sodium	340	Calcium	10.6
Cloride	340	Lactic acid	10
Phospholipids	280	Phosphate	4.5
Cholesterol	150	Magnesium	2.3
Bicarbonate	140	Uric acid	3
Neutral fat	125	Creatinine	1.5
Glucose	100	Bilirubin	0.5
Potassium	20	Bile salts	0.5
Urea	15	Else	4.9

Table 2.1: Average mass concentration of human blood plasma [127]

Name	Average cell concentration $[cells/ml]$	Approximate normal range $[cells/ml]$	Percentage of volume [%]
Erythrocytes	$4.8 \cdot 10^6$	$4.5 - 6.2 \cdot 10^6$	91
Leukocytes	$9.0 \cdot 10^3$	$4.1 - 10 \cdot 10^3$	5
Neutrophils	$5.4 \cdot 10^3$	$3.0 - 6.0 \cdot 10^3$	
Eosinophils	$2.7 \cdot 10^2$	$1.5 - 3.0 \cdot 10^2$	
Basophils	$6.0 \cdot 10^1$	$0 - 1.0 \cdot 10^1$	
Lymphocytes	$2.7 \cdot 10^3$	$1.5 - 4.0 \cdot 10^3$	
Monocytes	$5.4 \cdot 10^2$	$3.0 - 6.0 \cdot 10^3$	
Thrombocytes	$3.0 \cdot 10^5$	$1.5 - 4.0 \cdot 10^5$	4

Table 2.2: The size, percentage and the concentration of the main blood components [128]

The red blood cells are without nucleus, biconcave, disc-shaped bodies. From upper the shape is circle, an average diameter of the cell is 7.5 μm. Theirs number is around $4.5 - 6.2 \cdot 10^9$ $particles/dl$ [129]. The red blood cells are perfectly plastic structures, flexibly deformable, thus they can pass thought much smaller capillaries than their diameter. The shape of the red blood cells is sensitive to the osmotic variance. In hypotonic space (where the concentration of the salt is lower than 0.9 %) the shape of the cells change to spherical shape and after that the cells bursts and the hemoglobin flows out. In this case we get a hemolyzed solution with the hemoglobin and the membranes of the red blood cells.

The average cell concentration of leukocytes is around $4.1 - 10 \cdot 10^6$ $particles/dl$ [129]. The white blood cells are divided into several subclasses, for example basophils, eosinophils, lymphocytes, monocytes and neutrophils. These cells have a great wealth of form and functional character.

The platelets are ovoid, round, flat disc-shaped structures. These cell fragments haven't got nucleus, because they break away from the cytoplasm. The diameter of the platelets is 2-4 micrometers and the number of them is around $1.4-4.2 \cdot 10^8$ $particles/dl$ [129]. The platelets are responsible for blood clotting (coagulation), by converting fibrinogen into fibrin. This creates a mesh onto which red blood cells adhere and clot, which then stops more blood from leaving the body and also helps to prevent bacteria from entering the body.

Blood performs many important functions. First of all it transports oxygen to tissues. Blood supplies the cells with nutrients such as glucose, amino acids, and fatty acids, removes the waste (carbon dioxide, urea, and lactic acid). It has a messenger transport function with hormones and the signaling of tissue damage. The blood is supporting the body's self-repair mechanism with the coagulation functionality. The white blood cells make immunological detection functions of foreign material by antibodies. The blood makes the regulation of body pH (the normal pH of blood is in the range of 7.35 - 7.45). Also, it helps in the regulation of core body temperature.

2.2 Hemorheology and Hemodynamics

Hemodynamics is concerned with the mechanical and physiologic properties describing motion and equilibrium of blood flow under the action of external forces. Instead hemorheology describes the rheological properties of blood and its elements, such as morphology of blood cells and blood viscoelasticity. A full discussion of hemodynamic and hemorheology principles is beyond the scope of this thesis but in this chapter, an overview of basic principles is presented that are helpful in understanding the physical background.

2.2.1 Velocity and Pressure Profile of Blood Flow

The sample flow in microchannels has often been associated with negligible inertia that is, fluid flow in microfluidic channels is assumed to occur at low Reynolds number, where Reynolds number is a dimensionless parameter describing the ratio between inertial and viscous forces in a flow. The liquid flow is in streamline that is considered to consist of a series of thin laminae slipping over one another, meanwhile in turbulent case the blood moves in irregular varying paths continuously mixing within channels. The change of stream type form laminar to turbulent, which was introduced by Stokes, but measured by Reynolds, is described as:

$$Re = \frac{\rho D_H v}{\mu}, \tag{2.1}$$

which is also called Reynolds number, where ρ is the density of mass, D_H is the characteristic hydraulic diameter, v is the mean velocity of the object relative to the fluid, and μ is the dynamic viscosity. In a Stokes flow regime, where $Re \to 0$, the inertia of the fluid is ignored in most microfluidic platforms and contributions of fluid momentum are omitted from the NavierStokes equations resulting in linear, and thus time-reversible, equations of motion for Newtonian fluids. Practically achievable and useful flows in microfluidic systems could operate also in intermediate range flow ($\sim 1 <$Re$<\sim 100$) in which nonlinear and irreversible motions are observed for fluid and particles. The intermediate range flow regime, in which both the inertia and the viscosity of the fluid are finite, still lies within the realm of laminar flow which provides a deterministic nature and thus controllability of fluid and particles within. In the consideration of our

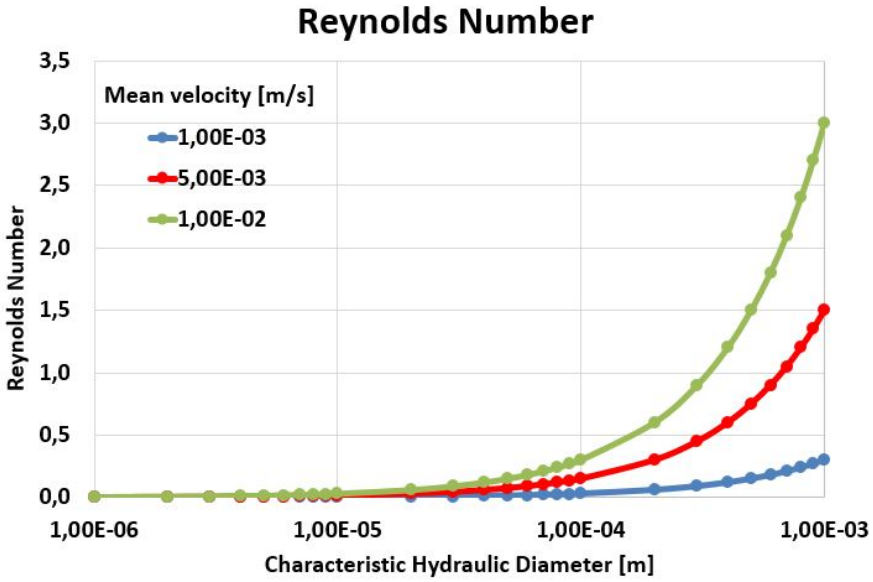

Figure 2.1: The Reynolds number of blood flow ($\rho = 1060\ kg/m^3$ and $\mu = 3.53{\cdot}10^{-3}\ Pas$) is calculated at different velocities (1 mm/s, 5 mm/s, and 10 mm/s)

application for blood with density of 1060 kg/m^3, shear viscosity of $3.53 \cdot 10^{-3}\ Pas$, the range of Reynolds number is shown in Fig. 2.1.

For case of low Reynolds number, neglecting inertia by using a Stokes flow approximation can lead to incorrect results. To determine the velocity and the pressure profile exactly in a microfluidic channel, the incompressible Navier-Stokes equation is applied assuming a constant viscosity (μ). The Navier-Stokes equation is derived from the basic assumptions of conservation of mass, momentum and energy in the following way:

$$\frac{\delta \vec{\mathbf{v}}}{\delta t} + \vec{\mathbf{v}} \cdot \nabla \vec{\mathbf{v}} = -\nabla P + \nu \nabla^2 \vec{\mathbf{v}} + F, \tag{2.2}$$

where $\vec{\mathbf{v}}$ is the velocity vector, P is the pressure and F is the sum of external body forces (gravity, electrophoretic forces, magnetophoretic forces, mechanical forces (i.e. ultrasound) and optophoretic forces).

2.2.2 Energy Conservation

Assuming no friction inside the flow, Bernoulli's equation can be developed from the Navier-Stokes equation (Eq. 2.2). Bernoulli's principle (conservation of energy) states that for an inviscid flow, an increase in the speed of the fluid occurs proportionately

with an increase in both its dynamic pressure and kinetic energy, and a decrease in its static pressure and potential energy, which can be described by the following way:

$$\frac{\Delta P}{\rho} + \frac{v^2}{2} + a_{grav}h = 0, \tag{2.3}$$

where ΔP is the pressure drop, a_{grav} is the acceleration due to gravity and h is height of fluid. This states that, in a steady flow, the sum of all forms of mechanical energy in a fluid along a streamline is the same at all points on that streamline, thus this requires that the sum of kinetic energy and potential energy remain constant.

2.2.3 Volumetric Flow Rate and Hydrodynamic Resistivity of Blood Flow

One of the properties of a fluid is that it will flow from a region of higher pressure toward a region of lower pressure. The primary parameter used in lab-on-a-chip devices to describe blood flow is the flow rate, which is the total volume of blood pumped through the channels per in a time interval. The relationship between blood flow, resistance, and pressure in cylindric channels can be determined using the Hagen-Poiseuille law:

$$Q = \frac{\Delta P \pi r^4}{8\mu L}, \tag{2.4}$$

where Q is the flow rate, ΔP is the pressure gradient, r is the radius of channel, μ is the viscosity of fluid (in our case: blood), L is the length of channel. Due to the blood is not a Newtonian fluid, the energy (and pressure) is lost as flowing blood overcomes resistance. The flow resistance can be considered in the following representation:

$$R = \frac{\mu L}{8\pi {D_H}^4}, \tag{2.5}$$

where D_H is the hydraulic diameter. Generally the length of microfluidic channels are few-millimeter long while the hydraulic diameter, which is a commonly used term when handling flow in noncircular tubes or channels, is defined by:

$$D_H = \frac{4A}{B}, \tag{2.6}$$

where A is the cross sectional area and B is the wetted perimeter of cross-section area. In microfabrication generally used microfluidic channels obtains rectangular cross-section shape, in this case the hydraulic diameter (D_H) can be considered the following way:

$$D_H = \frac{2wh}{w+h}, \tag{2.7}$$

where w is the width ($w \approx 100\mu m$) and h is the height ($h \approx 20\mu m$) of channel thus the typical value of the hydraulic diameter is around $33\mu m$. According to Eq. 2.4 the flow rate Q, which is determined by the pressure gradient, radius of channel, viscosity of fluid and length of the channel, is inversely proportional to the fluid resistance (Eq. 2.5) and it can be delivered such as:

$$Q = \frac{\Delta P}{R}. \tag{2.8}$$

In this case Eq. 2.4 can be considered analogous to the Ohm's law, hence the flow rate is inversely proportional to the resistance. The walls of the microfluidic channels are considered as rigid thus the Hagen-Poiseuille law is applicable. In the consideration of a 1 mm long straight microchannel with 20 μm depth and the width from 10 μm up to 300 μm the order of magnitude of flow resistance of blood flow is between $10^{10} - 10^{12}$ Pas/m^3, meanwhile the total pressure drop is in the range from few kPa up to the 100 kPa.

2.2.4 Kinematic Properties of the Blood Flow

In microfluidic channels, the flow is usually smooth and orderly because the fluid separates into an infinite number of concentric layers with different velocities. When a fluid (in our case: blood) flows past a solid surface, a thin layer develops adjacent to the surface where frictional forces retard the motion of the fluid. There is a gradient of frictional resistance between fluid in contact with the solid surface and fluid in the center of the stream. If the fluid particles travel along well-ordered nonintersecting layers, this is termed laminar flow. In a small Reynolds number case, the flouting particles are moved by the fluid through a viscous Stokes drag and their trajectories $X_p(t)$ [130]:

$$\frac{dX_p}{dt} = V_p, \tag{2.9}$$

$$\frac{dV_p}{dt} = -\frac{1}{\tau_p}\left[V_p - v(X_p, t)\right] + g, \tag{2.10}$$

where g is the acceleration of gravity, τ_p is the relaxation time of the particle, which is:

$$\tau_p = \frac{2\rho_p r_{particle}^2}{9\mu}, \tag{2.11}$$

where ρ_p is the mass density of the particle and $r_{particle}$ is the radius of the particle. The fluid velocity at the location of the particles is evaluated by linear interpolation. The particle inertia becomes dominant in higher velocity or mass.

Physical property	Blood	Water [131]	Parameter
Density (ρ)	$1.06 \cdot 10^3$ [132]	$1.0 \cdot 10^3$	$[kg/m^3]$
Shear viscosity (μ)	$3.53 \cdot 10^{-3}$ [133]	$1.0 \cdot 10^{-3}$	$[Pas]$
Kinematic viscosity (ν)	$3.33 \cdot 10^{-6}$ [134]	$1.0 \cdot 10^{-6}$	$[m^2/s]$
Surface tension (in air) (γ)	$5.8 \cdot 10^{-2}$ [135]	$7.3 \cdot 10^{-2}$	$[kg/s^2]$
PH	7.35-7.45 [136]	7	
hematocrit	45.7 [137]		[%]

Table 2.3: Physical properties of the human blood (at $37°C$) and water (at $20°C$) at 1 atm pressure

There are dimensionless numbers that gives information from the qualitative behavior of solute particles in a continuous single-phase liquid flow. The Reynolds number (Re) determines the inertial effect of fluid flow (turbulency), and the Péclet number (Pe) describes the mass transport contribution of molecules or particles (dispersion). The particle Reynolds number (Re_p) shows the inertial effect on a particle within a fluid flow, and the Stokes number (St) is useful to study the trajectory mismatch between the particle and fluid, and the size-based separation effect.

The particle Reynolds number (Re_p) can be defined as [138] and represented in Fig. 2.2:

$$Re_p = \frac{\rho v_{max} d_{particle}^2}{\mu D_H} = Re \frac{d_{particle}^2}{D_H^2}, \tag{2.12}$$

where Re is the Reynolds number, $d_{particle}$ is the particle diameter, v_{max} is the maximum flow velocity and μ is the shear viscosity (in our case, blood at $3.53 \cdot 10^{-03}$ Pas).

In the consideration of mass transport, the particle motion can be estimated by the Péclet number:

$$Pe = \frac{v_{maen} D_H}{D}, \tag{2.13}$$

where v_{mean} is the mean velocity of the fluid (in our case, $v \approx 1.0 \cdot 10^{-2}$ m/s) and D is the diffusion coefficient of particles. The diffusion coefficient of the particles is described by the Stokes-Einstein equation:

$$D = \frac{k_B T}{6\pi\mu r_{particle}}, \tag{2.14}$$

where k_B is Boltzmann's constant ($1.38 \cdot 10^{-23}$ J/K), T is the absolute temperature (in our case: 298 K), and $r_{particle}$ is the radius of the spherical particle. If Pe>1 the

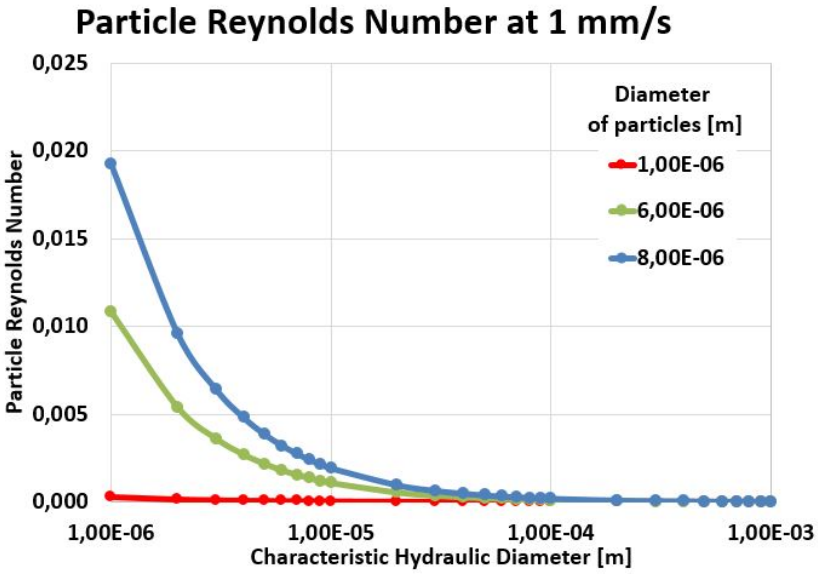

Figure 2.2: Particle Reynolds number of different size particles (1 μm, 5 μm, and 8 μm) at 1 mm/s flow rate within the blood ($\rho = 1060\ kg/m^3$ and $\mu = 3.53 \cdot 10^{-3}\ Pas$).

advection rate is bigger than the diffusion rate between rows of posts thus the particles are basically confined to streamlines. When a particle encounters an accelerating flow in a nonlinear channel, the Stokes number estimates the particle behavior as the ratio of the relaxation time of the particle (τ_p) (eq. 2.11) to the characteristic time of the flow (τ_f):

$$St = \frac{\tau_p}{\tau_f} = \frac{2\rho_p r_{particle}^2/9\mu}{D_H/v_{max}} = \frac{\rho_p}{18\rho} Re_p, \tag{2.15}$$

where v_{max} is the maximum fluid velocity well away from the obstacle, D_{post} is the characteristic diameter of the obstacle, ρ_p and ρ are the particle density and fluid density.

If St>1, a particle will continue in its original moving direction instead of following the fluid streamline when the flow turns suddenly by the channel geometry. The Péclet and the Stokes number of the main blood components at 0.001 mm/s flow rates are demonstrated in Fig. 2.3 and in Fig. 2.4.

2.2.5 Viscoelasticity of the Blood

Because blood is a non-Newtonian fluid, its rheological properties depend on shear rate and the dimensions and geometry of the conduit through which it flows. The cellular

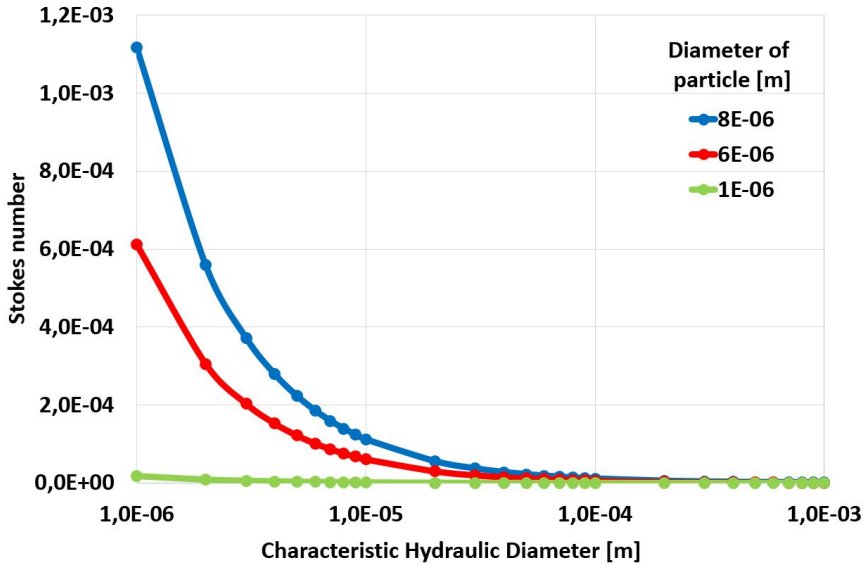

Figure 2.3: Péclet number of different size particles (1 μm, 5 μm, and 8 μm) at 1 mm/s flow rate within the blood ($\rho = 1060\ kg/m^3$ and $\mu = 3.53 \cdot 10^{-3}\ Pas$).

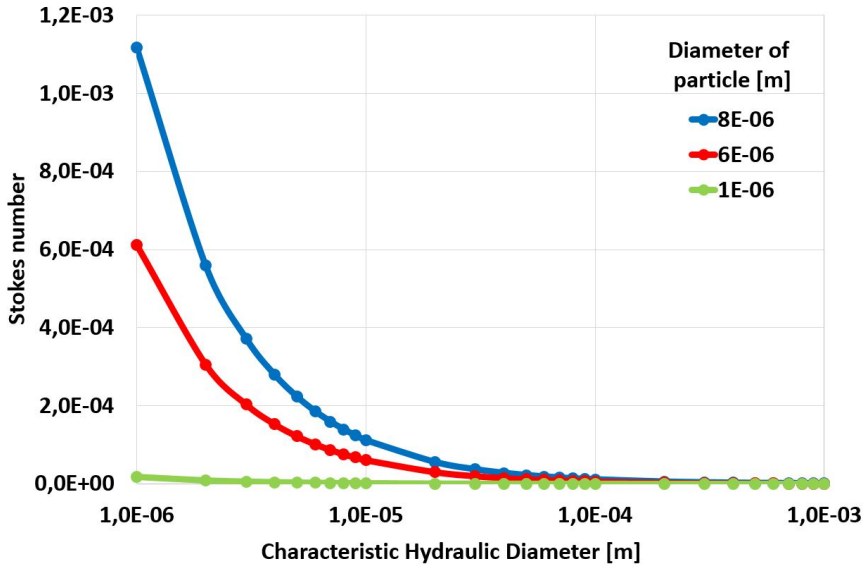

Figure 2.4: Stokes number of different size particles (1 μm, 5 μm, and 8 μm) at 1 mm/s flow rate within the blood ($\rho = 1060\ kg/m^3$ and $\mu = 3.53 \cdot 10^{-3}\ Pas$).

components are suspended in blood plasma, an aqueous solution that generally follows Newtonian dynamics. However, the two-phase nature of blood and the interactions between blood cells result in non-Newtonian dynamics, especially in the microchannels

where geometry dimensions become comparable to cell diameters. Because flow resistance is affected in many pathological conditions, quantitative approaches have been proposed to characterize the complex rheological properties of blood. A blood cells of flowing plasma will suffer forces from the surrounding fluid and walls, including viscous stress tensor (τ) that causes it to gradually deforms over time, which expresses how the element's deformation is changing with time. The rate of shear, also called velocity gradient, is caused by laminar flows along a channel that slip on one other and move in different speeds in a perpendicular direction to the wall of tube. If the ration between shearing stress and rate of shearing strain is linear the fluid is considered as Newtonian fluid. For an incompressible and isotropic Newtonian fluid, the viscous stress is related to the strain rate by the simpler equation:

$$\tau = \mu \frac{\delta v}{\delta y}, \tag{2.16}$$

where $\delta v/\delta y$ is the derivative of the velocity component that is parallel to the direction of shear, relative to displacement in the perpendicular direction. In respect of our application the liquid flow, which is vertebrate blood, is composed of blood cells suspended in blood plasma. The plasma, which constitutes 55 % of blood fluid, is an aqueous solution containing 92 % water, blood plasma proteins, dissolved nutrients (amino acids, fatty acids and glucose), waste products (carbon dioxide, urea, lactic acid) and other important component such as serum albumin, blood-clotting factors, immunoglobulins, lipoprotein particles, etc. [129]. In point of viscosity the intravenous blood cannot be considered such as a perfect Newtonian liquid due to floating blood cells, but the plasma. Viscoelasticity is a property of human blood that is primarily due to the elastic energy that is stored in the deformation of red blood cells as the heart pumps the blood through the body. The energy transferred to the blood by the pressure-driven flow is partially stored in the elastic structure, another part is dissipated by viscosity, and the remaining energy is stored in the kinetic motion of the blood. If the pressure pulsation is not significant of the pressure-driven flow is developed the elastic effect could be neglectable.

In Poiseuille flow, blood cells and plasma do not travel at the same average velocity. This results in differences in microchannels and discharge hematocrits. Although Eq. 2.4 is only valid for Newtonian fluids, fitting experimental data to this equation ($Q = \frac{\Delta P \pi r_{tube}^4}{8 \mu_e L}$) provides a convenient method of characterizing flow resistance by the

effective viscosity (μ_e), which depends on the fluid being tested, the capillary diameter, and the flow rate (or pressure drop) [139]. At high shear rate blood cells occupy the central axis of microfluidic channel leaving cell-free zone of plasma periphery. A decrease in haematocrit tends to increase shear stress due to the decreased effective viscosity (μ_e). The normal value of hematocrit is $40 - 45$ % for the man, meanwhile $35 - 40$ % for the women, which is approximately three times more that of water. Fåhræus-Lindquist effect [140] describes the relation between effective viscosity (μ_e) and the radius of capillary tubes (r_{tube}). According to experimental observation of Fåhræus et al. the relative viscosity of blood decreases inverse proportion to the diameter of channels due to the erythrocytes move over the center of the channel, leaving plasma at the wall of the microchannels and the hematocrit in the channel was always less than the hematocrit in the original sample. The ratio of these two hematocrits, the tube relative hematocrit (H_R):

$$H_R = \frac{hematocrit_{channel}}{hematocrit_{sample}}, \tag{2.17}$$

where $hematocrit_{channel}$ is defined as the ratio of blood cells volume within the channel to the total volume of the sample.

Chapter 3

Flow Through Nematodes Filter

3.1 Filtration of Nematodes Using an Integrated Microcapillary System

The filarial nematodes are a group of arthropod-borne worms that reside in the subcutaneous tissues, deep connective tissues, lymphatic system, or body cavities of humans. Some adult filarial worms can survive in the human host for many years, causing a number of chronic and debilitating symptoms, including inflammatory reactions [141]. The female worms produce large numbers of larvae called microfilariae, which are highly motile, threadlike prelarvae that in some species maintain the egg membrane as a sheath; these are called sheathed forms, while those that rupture the egg membrane are called unsheathed forms. Once released by the female worm, microfilariae can be detected in the peripheral blood or cutaneous tissues, depending on the species. The microfilariae, which may survive for 1 to 2 years, are not infective for other vertebrate hosts, nor do they undergo any further development in the vertebrate host [141]. The infections are transmitted to humans by the bites of obligate blood-sucking arthropods that had become infected through ingesting larvae (microfilariae) contained in a blood meal obtained from a mammalian host. The most speared filarial species in which the human is the definitive host is summed in Tab. 3.1.

Disease-specific immunodiagnostic and molecular testing markets increase worldwide. The genus *Dirofilaria*, which includes etiologic agents such as *Dirofilaria immitis* and *Dirofilaria repens*, is responsible for the increased occurrence of zoonotic dirofilariosis in vertebrates worldwide. Human infections by these parasites may also occur,

Species	Distribution	Vector	Location
Wuchereria bancrofti	Tropics and subtropics worldwide; mainly India, China, Indonesia, Eastern Pacific	Mosquito	Lymphatic
Brugia malayi	Southeast Asia, Indonesia, India, Indonesia, Southeast Asia	Mosquito	Lymphatic
Brugia timori	Islands of Timor and Lesser Sunda in Indonesia	Mosquito	Lymphatic
Loa loa	Africa	Deerfly	Subcutaneous
Mansonella perstans	South and Central America, Africa	Biting midge	Body cavities, mesentery, perirenal
Mansonella ozzardi	South and Central America, Caribbean	Biting midge, blackfly	Subcutaneous, body cavities
Mansonella streptocerca	West and Central Africa	Biting midge	Subcutaneous
Onchocerca volvulus	South and Central America, Africa	Blackfly	Subcutaneous
Dirofilaria immitis	Japan, Australia, United States, Europe	Mosquito	Pulmonary nodules
Dirofilaria repens	United States, Africa, Asia, Europe, and South America	Mosquito	Subcutaneous

Table 3.1: Listing of human filariasis by Gracia et al. [141]

and 1782 cases have been reported in over 37 countries in Europe, North America, Southeast Asia, and Africa [142–144], 372 of which were pulmonary and 1410 of which were subcutaneous/ocular cases over the last decade [145]. Increased -travel, pesticide -restrictions, and the introduction of the Asian tiger mosquito, which take a blood -meal that is twice as large as the common mosquito species, have contributed to the spread of cardiopulmonary and subcutaneous dirofilariosis in final host carnivores [146].

The life cycle of species of *Dirofilaria* genus consists of larval stages (L1-L3) in arthropod intermediate host as vector (mosquito), developing stages (L3-L5) and adult

stage in natural host (Fig. 3.1). The development period of the microfilariae mostly depends on the temperature inside the species of intermediate host (from 10 to 21 days at around $25°C$). In infective stage, the larvae (L3) migrate to the Malpighian tubule lumen of the mosquito, while during subsequent nutrition of the intermediate host the larvae enter to subcutaneous connective tissue of definitive host. In this stage (L3), the infective larvae of these filarioidea invade a variety of human or animal tissues and elicit little or no discernible response from the host during the course of their development unless they enter exquisitely sensitive tissues such as the conjunctivae. The *D. immitis* and *D. repens*, which are responsible in human, persist for months without a detectable host response. In their natural hosts, filarioids are typically long-lived, living often several years or more [147]. *D. immitis* infective larvae (L3s), commonly called "heartworm", cause a chronic infection in the right heart/inferior vena cava, and the pulmonary vein where uncontrolled parasite development may result in serious disease for the natural host but in humans do not survive their migration in subcutaneous tissue [148]. *D. repens* causes chronic infection where parasite development is limited within the eye, subcutaneous tissues, abdominal cavities, and urinary bladder. Species of *Dirofilaria* affect mostly dogs and other carnivores such as cats, wolves, and foxes. Humans may become infected as aberrant hosts, the worms fail to reach adult stage while residing in a human body.

The late stage (L4-L5) differential diagnosis of human pulmonary dirofilariosis costs $80,000 or more per patient in the USA [160]. In addition, in the case of *D. immitis*, it exposes the patient to unnecessary surgery which carries a risk of mortality. Therefore, the early-stage (L3) diagnostic techniques reduce risk of complications and also save health care costs. Large scale screening for dirofilariosis involves the use of the serologically based antigen or antibody lateral flow devices which are commercially available for this purpose: VetScan Canine Heartworm Rapid Test Kit (Abaxis, Union City, CA, USA), Heartworm IC (Argolabo S.p.A., Scarmagno, TO, Italy), Solo Step CH Canine Heartworm Antigen Test (Heska, Loveland, CO, USA), FASTest HW Antigen (Megacor Diagnostik GmbH, Hoerbranz, Austria), CH9705/FX Immunochromatographic device (Multimage S.r.l., Cavaria, VA, Italy), Woodley InSight Heartworm Rapid Diagnostic Test (Woodley Equipment Company Ltd, Horwich, UK), and Canine Heartworm Antigen Test (SA Scientific, San Antonio, TX, USA). These antigen or antibody lateral

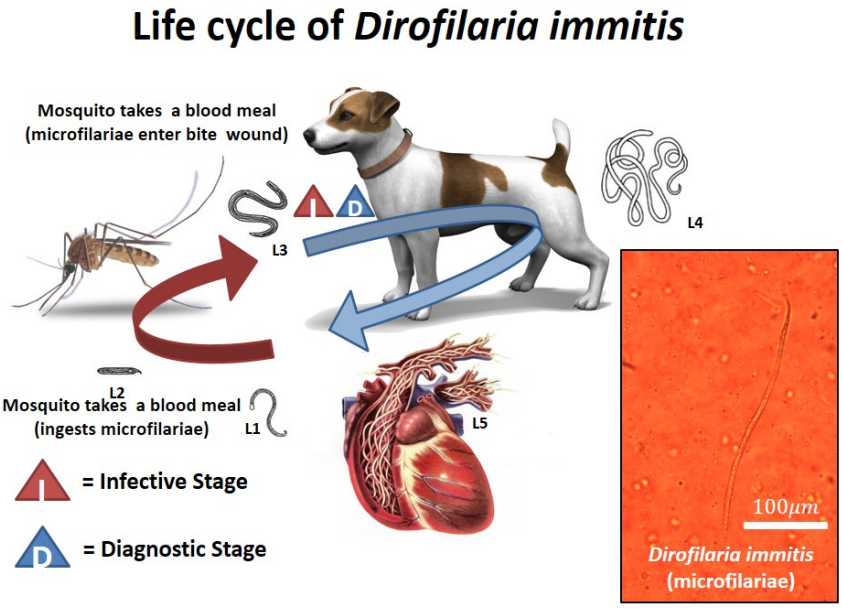

Figure 3.1: The life cycle of *Dirofilaria immitis* which consists of three stages (L1-L3) in arthropod (mosquito) intermediate vector and other two stages (L4 and L5) in vertebrate host. During the blood meal, an infected mosquito introduces L3 filarioid larvae of *D. immitis* into the skin of the definitive host. The L3 nematodes invade the tissues of natural host undergoing themselves two more molts into adults. Adult heartworms reside in pulmonary arteries and are occasionally found in the right ventricle of the heart. Adult females are usually $250 - 310$ mm long by 1 mm wide; males are usually $120 - 200$ mm long by $0.7 - 0.9$ mm wide. Adults can live for $5 - 10$ years. In the heart, the female worms are capable of producing microfilariae over their lifespan, which are $290 - 330$ μm long and $5 - 7$ μm wide [149]. The microfilariae are found in peripheral blood, which can be ingested by another mosquito during its blood meal.

flow devices require at least three adult female heartworms and do not exist for detection of *D. repens*. The antigen presence of dirofilariosis does not occur in each case thus in diagnostics several seroepidemiological methods have been developed to explore the existence of intravenous nematodes or to determine its volumetric population from blood samples. The gold standard in diagnosis depends upon microscopical detection of microfilariae in blood but classical microbiological test is also used. This is very difficult in dirofilariosis where the parasitemia is frequently below 100 nematodes per milliliter of blood. Given the low abundance of parasites in the blood, methods have been developed to raise the efficiency of detection rising the cost and the required time

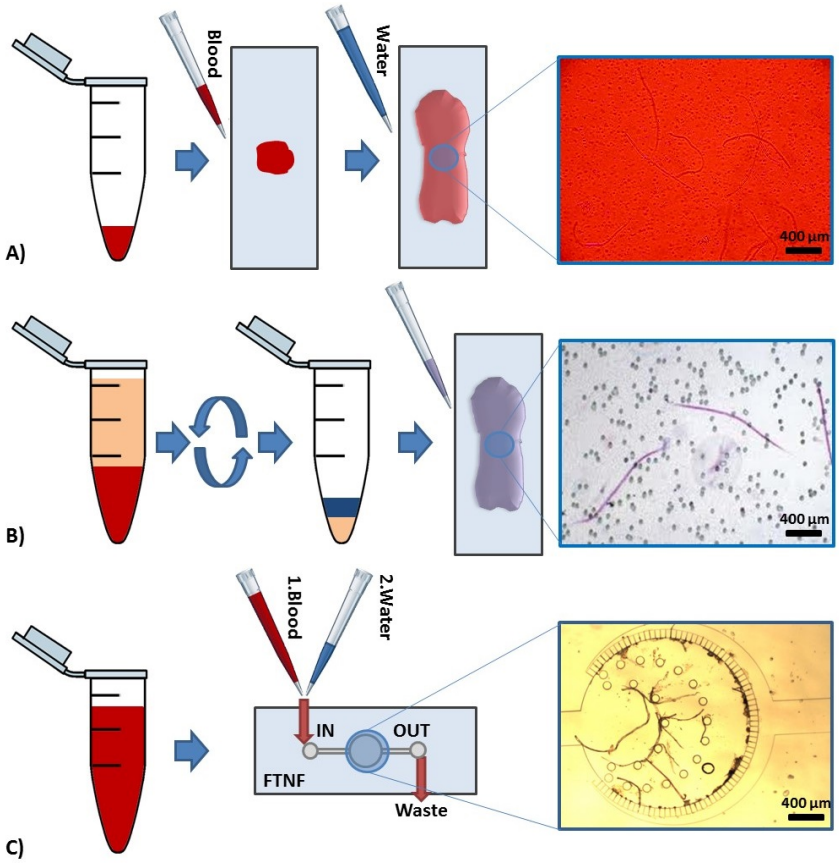

Figure 3.2: A) Blood smear test. Starts with pipetting a drop of serological sample on a glass slide, then hemolysing with deionized water and finally counting the number of nematodes within the all volume of sample. B) The modified Knott′s test. Anticoagulant blood sample is dissolved 2% formalin in a conical centrifuge tube. After the 5 minutes centrifugation at 1500 *rpm*, the sediment is mixed by one drop of methylene blue stain coloring the cuticle of nematodes. Finally, the number of nematodes is counted optically. C) Flow-through nematode filter (FTNF). Concentrates the nematodes in the center of the device before the hemolysis from few *ml* of blood offering an instantaneous readout.

of diagnosis. The following enumeration, which is also summarized in Table 3.2, represents a scale of executive complexity in inverse proportion of currently used diagnostic methods [146]: serologic methods (fresh blood smear and histochemical stain based tests), concentration methods (Knott's test, hematocrit method, filter test), enzyme-linked immunosorbent assays (ELISAs), multiplex real-time PCR amplification. When dirofilariosis is diagnosed, the erratic progression of many infections and the lack of microfilariae in most cases necessitate the use of combined diagnostic techniques. The

Method	Limit of detection	Volume requirement	Duration	References
Serologic methods (fresh blood smear, histochemical stain based tests)	1-2 nematodes	0.5-1 ml	10-30 min	[146, 150]
Concentration methods (Knott's test, hematocrit method, filter test)	1-2 nematodes	2-3 ml	20-40 min	[151, 152]
Enzyme-linked immunosorbent assays (ELISAs)	22-43 kDa antigens	200-400 μl	2-4 h	[153–156]
PCR amplification	2-3 DNS	10-100 μl	3-5 h	[142, 157–159]

Table 3.2: Laboratory diagnostics of blood-borne parasitic diseases

evaluation of serological methods and the concentration procedures are based on optical detection while the enzyme-linked immunosorbent assays (ELISAs) and RT-PCR amplification requires further costs (instruments, higher skilled labor). Each diagnostic technique is multiplexable and combinable with other methods. The most simplest and speared technique is the smear test, which is shown in Fig. 3.2.A and starts with pipetting serological sample onto a glass slide after the hemolysis, the nematodes are counted. The modified Knott's test, which concentrates nematodes by centrifuge and mark specific species by Giemsa stain and shown in Fig. 3.2.B. First, the anticoagulant blood sample is dissolved 2% formalin in a conical centrifuge tube. After the 5 minutes centrifugation at 1500 *rpm*, the sediment is mixed by one drop of methylene blue stain coloring the cuticle of nematodes to distinguish better the different nematode spices. Finally, the number of nematodes is counted as the previous method. The advantage of the concentration method versus the basic serologic methods is raised detection limit from a bigger sample volume. The presented microfluidic device (flow-through nematode filter, FTNF), which is shown in Fig. 3.2.C uses an integrated filtering technique providing the ability to detect much smaller concentration of nematodes from specimens, determine them more accurately and specifically without any external devices reducing the price of the measurement approximately at same efficiency.

The our developed diagnostic device integrates a flow-through nematode filter (FTNF) to concentrate circulating parasites from serological sample. The overall mechanism and the novelty of the developed device is shown and highlighted in Fig. 3.2.B. The designed biochip contains a microfluidics-based particle separation technique which is easy to implement in cheap disposable plastic chips, that we believe is well suited for the task of removing parasites from few ml of blood in order to aid the instantaneous detection. The mechanism of separation by FTNF is based on the interaction of nematodes suspended in whole blood with an ordered array of microcapillaries that the fluid is forced to flow through under low Reynolds number conditions, while the detectable larvae are trapped.

The required filtration range of the designed device for nematode filtration comes from parasitology. These nematodes are ovoviviparous and the evolving unsheathed embryo (microfilariae) live in the bloodstream. The length of *D. immitis* is $330-380\ \mu m$ and their width is $5-7\ \mu m$ [149]. The microfilariae of *D. repens* is bigger, $300-360\ \mu m$ long and $6-8\ \mu m$ wide [149]. In this matter the developed structure has to be robust, efficiently filter out the desired nematodes and reduces the risk of coagulation.

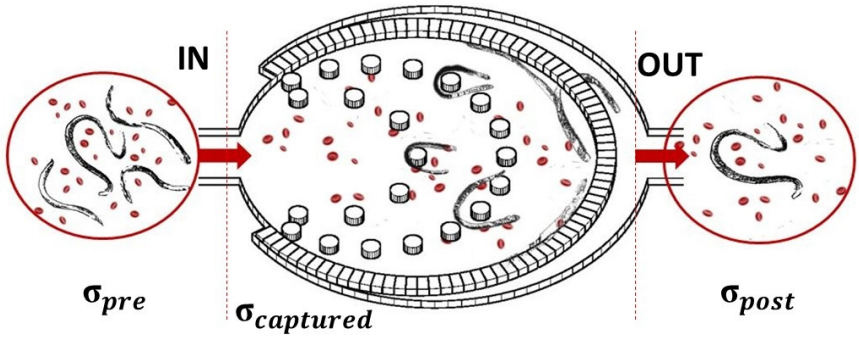

Figure 3.3: The overall mechanism of the flow through nematode filter (FTNF) device. Parasite-infected serological sample is forced through the capillary system, meanwhile the mayor part of them are remained trapped.

Here, a continuous hydrophoretic filtration technique of nematodes which does not require auxiliary liquid control, can be fabricated using a monolithic polydimethylsiloxane (PDMS)-glass technique and solve the described purpose, has been presented to construct 12 parallel microfluidic systems changing microcapillary width from 6.1 μm up to 15.4 μm. The developed flow-through nematode filter (FTNF), which represented

in Fig. 3.3 is is based on a common microfluidics-based particle filtration technique, easy to implement in cheap disposable plastic chips, that we believe is well suited for the task of removing parasites from blood in order to aid detection. The mechanism of separation by FTNF is based on the interaction of nematodes suspended in whole blood with an ordered array of microcapillaries that the fluid is forced to flow through under low Reynolds number conditions, while the detectable larvae are trapped. The fabrication of constructed devices are based on soft-lithography techniques using monolithic polydimethylsiloxane (PDMS).

3.2 Device Principles

Figure 3.4 demonstrates the geometry of the developed microfluidic filter for this mentioned veterinarian purpose. Each microfluidic structures has one 400 μm wide and 20 μm high inlet and one outlet. 12 capillary structures have been implemented, which are uniform within the central region of one device but the widths of microcapillaries ($W_{capillary}$) varies from 6.1 μm up to 15.4 μm. The active zone, where parasites remain trapped is surrounded by these rectangular cross-section microcapillaries, which are on a radius (r) of 1 mm from the center and its repetition angle (α) is from 3.38° up to 3.91°. The width of obstacles/pillars (W_{pillar} = 52.8 μm) and the angle without capillary connection ($\beta = 75°$) are the same in each structure.

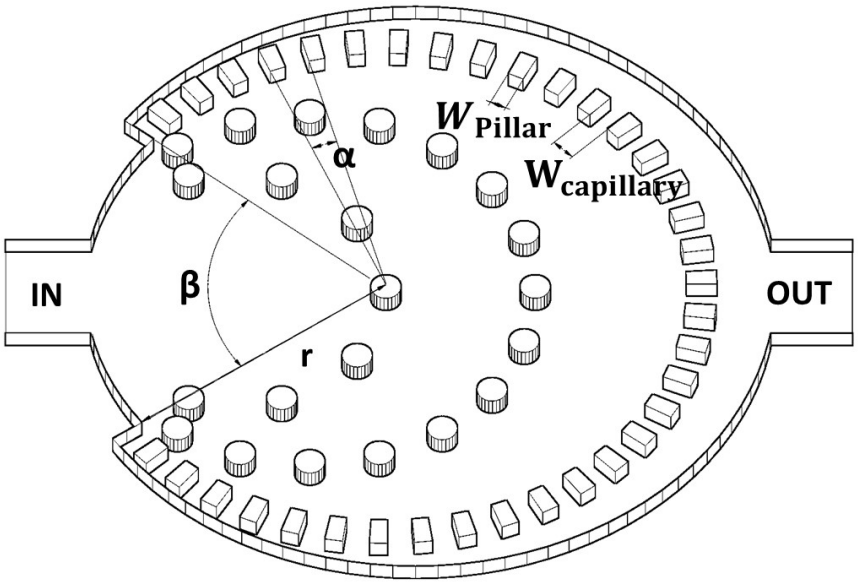

Figure 3.4: Schematic of the developed flow-through nematode filter. The α angle is the structural repetition of the microcapillaries, r is the radius of the active zone, W_{pillar} is the width of the pillars, $W_{capillary}$ is the width of the capillary channel and β is the angle without capillary connection.

The following trigonometrical equations describe the relationship between α and

the capillary width ($W_{capillary}$):

$$\sin\frac{\alpha}{2} = \frac{W_{pillar} + W_{capillary}}{2r} \tag{3.1}$$

$$W_{capillary} = 2r\sin\frac{\alpha}{2} - W_{pillar} \tag{3.2}$$

Those rigid particles which have greater diameter than $W_{capillary}$, will be filtered out from the liquid flow. The total cross section of microcapillaries is described by the following equation:

$$S_{capillaries} = \frac{\beta h}{\alpha}(2r\sin\frac{\alpha}{2} - W_{pillar}) \tag{3.3}$$

where h is the height of channel and $360° - \beta$ is that angle where the capillaries connect to the active zone along.

Generally, the microfluidic filters are described by the pressure drops (ΔP) at different flow velocities and the total flow resistance (R_{tot}).

$$\Delta P = R_{tot}Q \tag{3.4}$$

The pressure drop is the function of the flow rate (Q) and the total flow resistance R_{tot} which is defined as:

$$\frac{1}{R_{tot}} = \sum_{i=1}^{n}\frac{1}{R_i} = \frac{1}{R_1} + \frac{1}{R_2} + ... + \frac{1}{R_n} \tag{3.5}$$

where n is the number of capillaries within one device ($n = (360° - \beta)/\alpha$). R_i is the flow resistance of one capillary channel

$$R_i = \frac{8\mu L}{\pi r_H^4} \tag{3.6}$$

where μ is the dynamic viscosity, L is the length of the microcapillary and the nominal hydrodynamic diameter (r_H) is

$$r_H = \frac{hW_{capillary}}{h + W_{capillary}} \tag{3.7}$$

Integrate Eq. 3.5, Eq. 3.6 and Eq. 3.7 into Eq. 3.4 we get the pressure drop of cylindric-shape capillary structure

$$\Delta P = \frac{8\mu LQ\alpha(h^4 + W_{capillary}^4)}{\pi\beta h^4 W_{capillary}^4} \tag{3.8}$$

The calculated results are shown in Fig. 3.6.

3.3 Computational Fluid Dynamic Simulations

In order to provide efficiency of filtration, computational fluid dynamics simulations were calculated to predict the velocity and pressure profiles of the developed structure by COMSOL Multiphysics 4.3 (COMSOL Inc., Burlington, MA, USA). The pressure drop has a significant meaning in the point of flow through filtering. 12 similar microfluidic devices were designed by increasing capillary width ($W_{capillary}$) from 6.1 μm up to 15.4 μm and the flow velocity and pressure profile was calculated at 0.25 ml/h, 0.5 ml/h, and 1 ml/h flow rates with the initial and boundary condition and shown in Fig. 3.5.

The initial parameters were set to the average blood properties thus the viscosity was around $3.53{\cdot}10^{-3}$ Pas, the density was 1060 kg/m^3 in the all domain of microfluidic device. On the walls were set non slipping condition, on the outlet to zero-pressure and on the inlet laminar inflow condition at 0.25 ml/h, 0.5 ml/h, and 1 ml/h volumetric flow rates. To investigate the efficiency of filtration the pressure drop has a important effect. If the pressure drop is significant the trapped elastic particles, which are larger than the capillary width ($W_{capillary}$) can be squeezed through the microcapillary structure while using an abnormal pressure the filter can be also destroyed [161].

For each geometry the flow velocity and pressure profiles have been calculated and the maximum pressure differences within the devices are shown in Fig. 3.6. The pressure field has a maximum value on the sidewall of inlet and the smallest value appears on the sidewall of outlet. Within one device the pressure drop raises in a laminar way in the function of flow rate and reduced by the capillary width at the same boundary and initial conditions. The equidistant microcapillaries from the geometric center develop a quasi-homogeneous pressure field within the active zone, which is the central field of the microfluidic device, where the nematodes remain trapped, aiding the filtration of the larvae but blood cells. Based on computational flow dynamics simulations the approximation of the pressure drop can describe with the following equation with $R^2 = 0.9939$:

Decreasing the capillary width ($W_{capillary}$) increases the flow resistance quasi exponentially and in the same time the pressure drop at a fixed flow rate which is represented

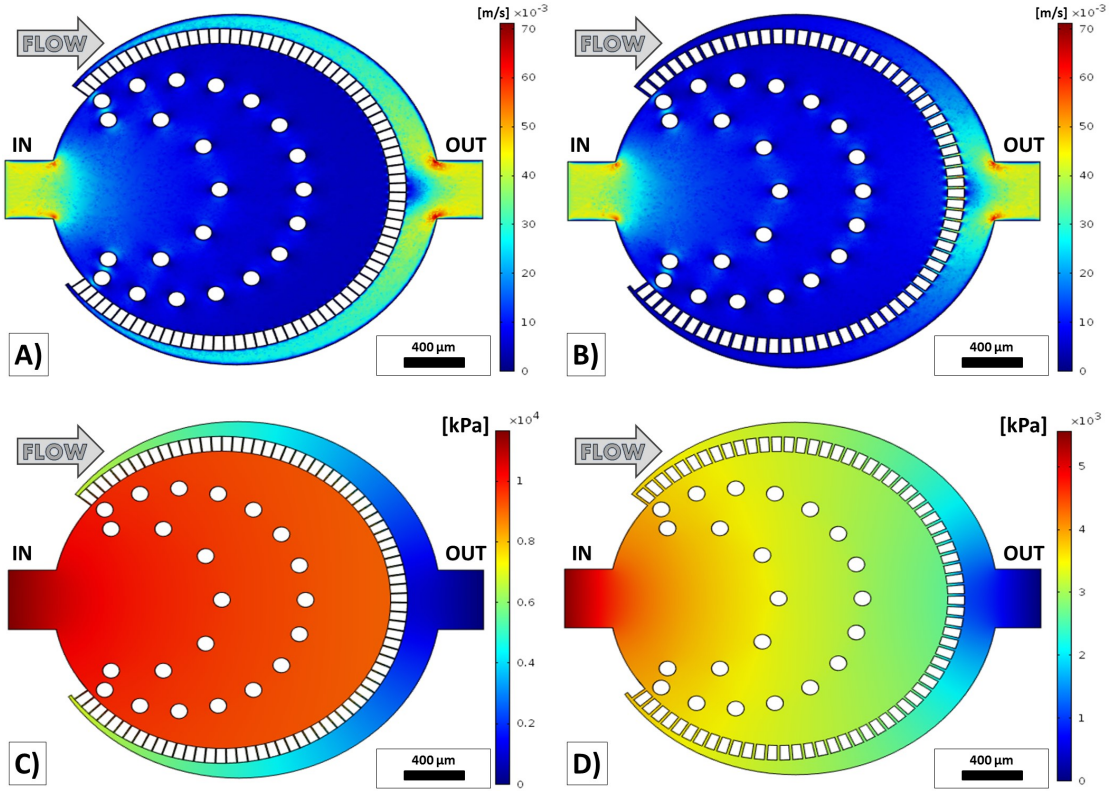

Figure 3.5: Flow velocity and pressure profiles at 1 ml/h. A) Flow velocity profile of the thinnest ($W_{capillary} = 6.1\ \mu m$) capillary structure at 1 ml/h. B) Flow velocity profile of the thickest ($W_{capillary} = 15.4\ \mu m$) capillary structure at 1 ml/h. C) Pressure profile of the thinnest capillary structure at 1 ml/h. D) Pressure profile of the thickest capillary structure at 1 ml/h.

in Fig. 3.6.

3.4 Device Design and Fabrication

Channel layouts were designed by using AutoCAD 2013 (Autodesk Inc., San Rafael, CA, USA) and devices were fabricated in polydimethylsiloxane polymer (PDMS, Sylgard 184, Dow Corning, USA) using a standard microfabrication soft-lithographic techniques [161]. The microfabrication procedure starts with making a master for replica molding. SU-8 (MicroChem, Newton, MA, USA) photoresist was spin coated onto 4" silicon wafer to a thickness of 20 μm and patterned using UV light in contact mask

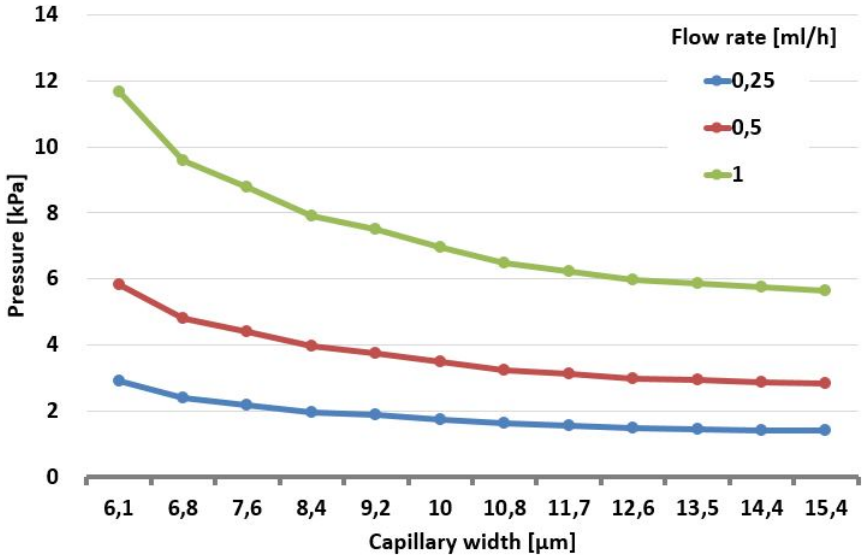

Figure 3.6: Pressure drop within each device calculated by computational fluid dynamics simulations at 0.25 ml/h, 0.5 ml/h, and 1 ml/h flow rates.

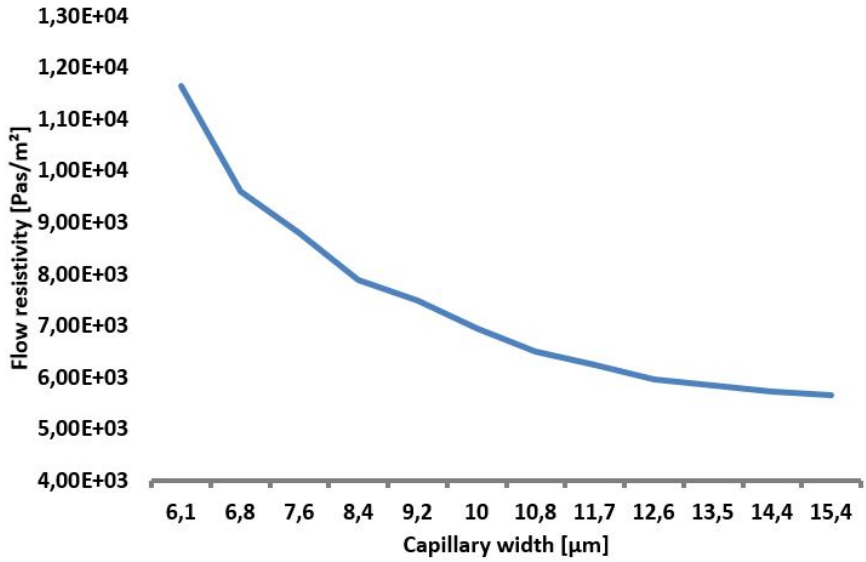

Figure 3.7: Flow resistivity within each device calculated by computational fluid dynamics simulations.

aligner through a chrome mask. PDMS monomer and curing agent (Sylgard 184, Dow Corning, Midland, MI, USA) were mixed to a ratio of 10 : 1 (v/v), degassed and poured over the master and set aside at 70°C for 2 h for polymerization. The liquid PDMS pre-

polymer conforms to the shape of the master and replicates the features of the master. After the polymerization the solid PDMS replica was lifted off from the mold surface and access holes were punched through the patterned PDMS slab using a 1 mm hollow pin vise. The patterned PDMS slab was bonded to microscope glass slide following surface treatment by Plasma-preen II 863 (Plasmatic Systems Inc. North Brunswick, NJ, USA). Finally, teflon tubes were inserted into the access holes for fluidic contacts.

3.5 Experimental Setup

Figure 3.8 illustrates the schematic diagram of our nematode detection platform. Pressure-driven flow was created using syringe pumps (NE-4000, New Era Pumping System Inc, Farmingdale, NY, USA) attached to the inlet via Teflon tubes, which made it possible to hydrodynamically focus the sample into a stream of 20 μm in width. Typical flow rates were used between 0.1 ml/h and 2 ml/h, controlled by the syringe pump. Imaging was performed on an inverted Olympus IX71 microscope (Olympus, Tokyo, Japan). Image recording was through a USB color CCD camera (uEye UI-222x series, IDS Imaging Development Systems GmbH, Obersulm, Germany). All videos were captured at a speed of 50 frames/second and captured videos were analyzed by using Matlab (The MathWorks Inc., Novi, MI, USA). For parasitological experiments, blood-borne infected, anticoagulant, canine blood has been used, where *D. repens* parasites were determined previously by Knott's method obtaining their concentration in serological samples.

3.6 Experimental Results

The single layer microfluidic design allows the easy loading, immediate detection and analysis of nematodes, eliminating the need of other sample preparation instruments such as centrifuge or devices. Before each experiment, these microfluidic structures were optically checked, purified and dried avoiding unnecessary particles (dust), which can cause clogging. The developed structure were tested at at 0.25 ml/h, 0.5 ml/h, and 1 ml/h volumetric flow rates by 15 different blood-borne infected, anticoagulant, canine blood samples. The type and the severity of dirofilariosis was determined and classified into three classes (-, +, ++).

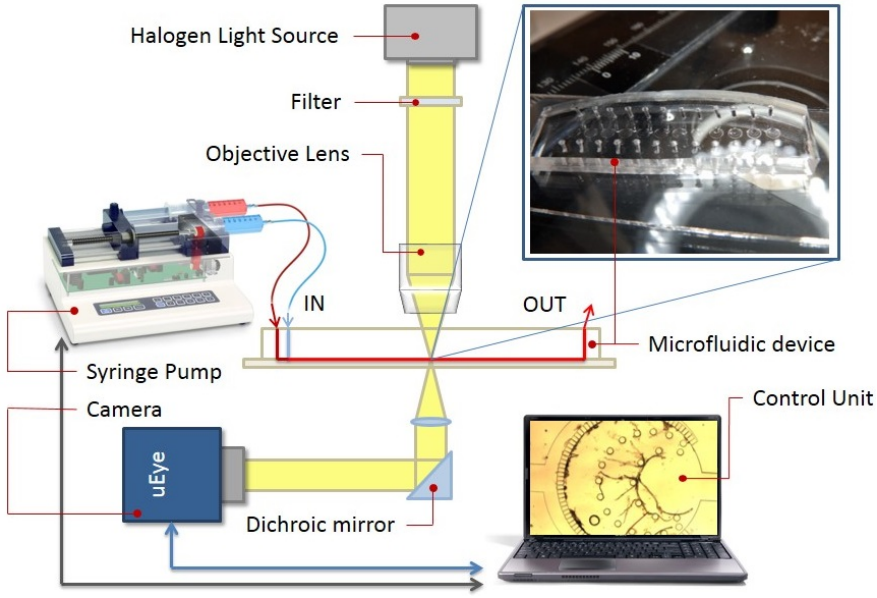

Figure 3.8: Schematic image from the developed parasite detection platform. The microfluidic devices are mounted on an inverted phase contrast microscope. The syringe pump system with the CCD camera unit are controlled via a common platform.

Figure 3.9 shows the developed procedure of nematode detection, which contains the following steps. Firstly, the serological sample is forced through the microfluidic device at a constant volumetric flow rate meanwhile the major part of the nematodes remained trapped in the isobaric central region (Fig. 3.9.A). Changing the medium to deionized water, air bubble is pushed thought the capillary structure additionally (Fig. 3.9.B). Due to the deionized water induces hemolysis by osmotic shock the attached and aggregated cells as thrombocytes and lymphocytes are lysed and flushed away from the detection area, meanwhile nematodes are resistant to osmotic shock thanks to its cuticulae which increases the visibility is increased by rising the contrast (Fig. 3.9.C). Finally trapped nematodes are counted optically in the central region (Fig. 3.9.D). The experiments indicates that the number of trapped nematodes correlates with the applied volumetric flow rate and the applied microcapillary width.

Blood-borne infected, anticoagulant blood samples were pushed through the biochips and the major population of nematodes remain captured in the quasi-isobaric central region (Fig. 3.4.A). The population of the nematodes in the original blood samples (σ_{pre} and in the waste products (σ_{post}) were analyzed by basic serologic methods (tick blood

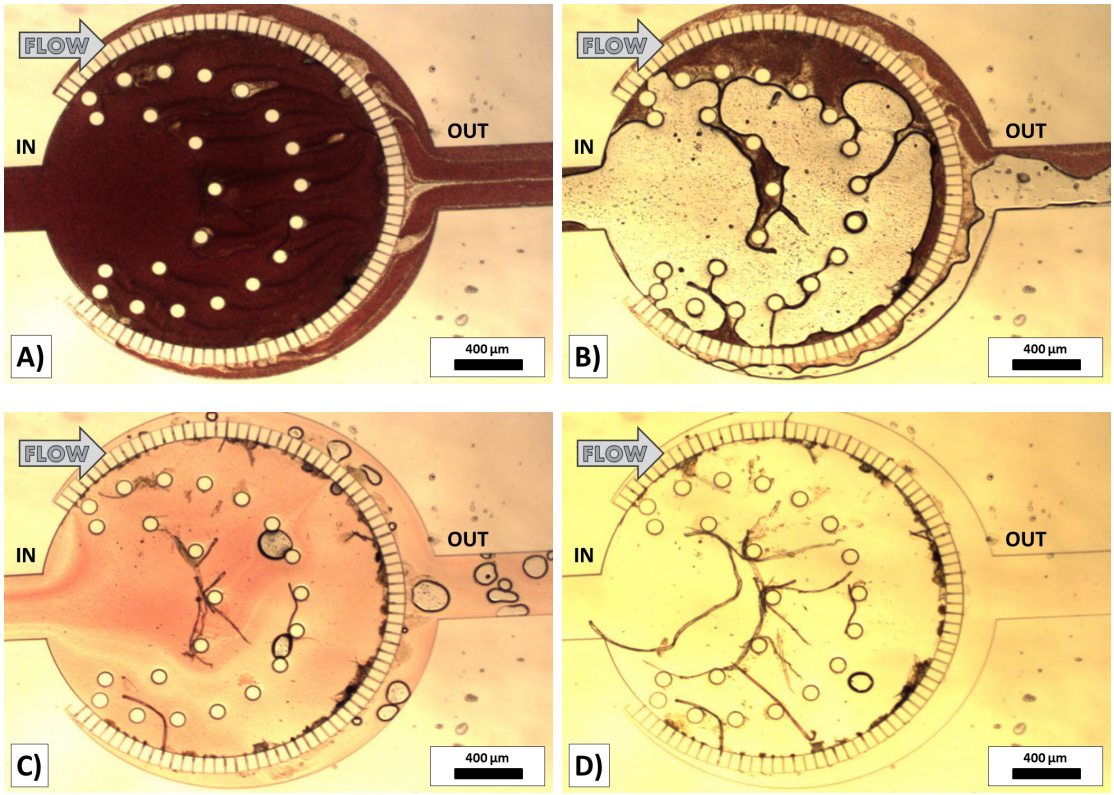

Figure 3.9: Developed procedure of nematode detection. A) serological sample is forced through the microfluidic device B) the medium is changed to air then deionized water C) haemolysis and increment of visibility D) counting the nematodes optically

smears) to determine the efficiency of the device at different flow rates (0.25 ml/h, 0.5 ml/h, and 1 ml/h). The filtration efficiency (η), which represented on Fig. 3.4.A, has been calculated by taking the ratio of the trapped nematodes ($\sigma_{captured}$) and the initial volumetric concentration of larvae (σ_{pre}) in the native serological sample. The number of trapped nematodes ($\sigma_{captured}$) has been counted optically within the active zone. Obtaining a homogenous sample the following equations were reached:

$$\sigma_{pre} = \sigma_{captured} + \sigma_{post} \tag{3.9}$$

In the sense of sample volume is fixed and concentration is homogeneous the efficiency (η) can be defined by the following way:

$$\eta = \frac{\sigma_{captured}}{\sigma_{post} + \sigma_{captured}} \tag{3.10}$$

Due to the sedimentation of the heavier particles (nematodes), inhomogeneity (IH) of the serological sample can be occurred at low flow rates, which can cause false prediction of the nematodes population in the original sample. The inhomogeneity of the samples was defined by the following equation:

$$IH = \frac{|\sigma_{pre} - \sigma_{captured} + \sigma_{post}|}{\sigma_{pre}} \tag{3.11}$$

The efficiencies of the different microfluidic channels, which is presented in Fig. 3.10, have been calculated at constant volumetric flow rates (0.25 ml/h, 0.5 ml/h, and 1 ml/h) by the previously described procedure. During each measurement, one examined sample (+ or ++) was chosen and forced through 12 different FTNF structures with microcapillary width from 6.1 μm up to 15.4 μm separately at constant flow rate five times binning efficiency (η) for histograms. The average population of the nematodes in the original blood samples (σ_{pre}) was obtained from 5 intermediate control tests at each measurement. The volumetric nematode concentration (σ_{pre}) was between $0.65 \cdot 10^3$ and $3.06 \cdot 10^3$ $nematodes/ml$). The flow velocity on the inlet determines the pressure drop though the microcapillary structure. Rising the flow rate, the pressure drop forces more nematodes through the filter decreasing the efficiency of the filtration. In the other hand, decreasing flow rate has an influence on the inhomogeneity of the samples. Optimizing the applied flow rate for the described purpose, the inhomogeneity was also measured and binned for histograms. The standard deviations of the mean values of filtration efficiency and sample inhomogeneity were counted and displayed on Fig. 3.10 with trendlines and theirs R-squared values. The robustness analysis of the procedure was considered by trend estimation of mean efficiencies of different devices ($W_{capillary}$ from 6.1 μm up to 15.4 μm) and its R-squared values ($R^2 = 0.8996$ at 0.25 ml/h, $R^2 = 0.9829$ at 0.5 ml/h and $R^2 = 0.7506$ at 1 ml/h). The highest mean efficiency of filtration was obtained at 0.5 ml/h flow velocity with the best trend fit. Based on the measurements, we found that increasing flow rate increases the level and the stability of homogeneity. Decreasing capillary width ($W_{capillary}$) the filtration efficiency rises but applying a higher volumetric velocity the nematodes can be forced through the capillary structure due to the raised pressure drop and the properties

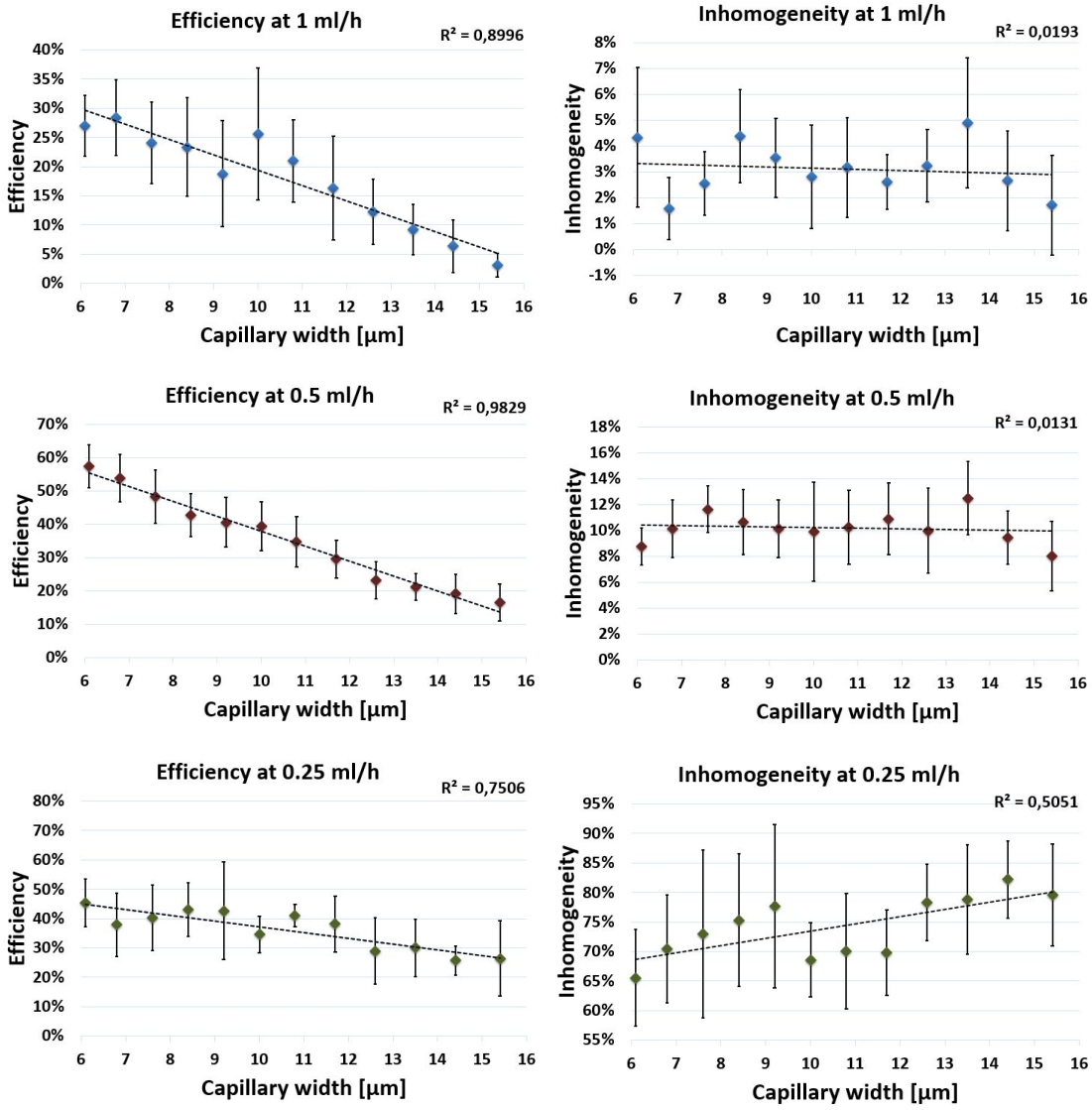

Figure 3.10: The efficiency and the inhomogeneity of each microfluidic structure ($W_{capillary}$ from 6.1 μm up to 15.4 μm) at different flow rates (0.25 ml/h, 0.5 ml/h, and 1 ml/h). The error bars of each histogram shows the standard deviations from the mean values. The R-squared values of each trendlines are displayed.

of non-rigid particles. Finally, we found that the best setup was using 6.1 μm wide capillary at 0.5 ml/h flow rate.

The classical veterinarian procedures includes sedimentation or centrifugation just for sample preparation and the total procedure time takes $30 - 45$ $mins$ without guar-

antee the homogeneity of concentration of nematodes [146]. The pushed-through of 0.01 ml of samples through the developed biochips at 0.25 ml/h volumetric flow rate takes 58 $mins$, at 0.5 ml/h takes 29 $mins$ and at 1 ml/h takes 15 $mins$ which is comparable with the widely used nematode diagnostic procedures (Table 3.2). The parallelization of the measurement reduces the procedure time guaranteeing the same filtration efficiency.

3.7 Results with the Flow Through Nematode Filter

I have successfully shown how microfilariae circulating in the blood stream can be detected using the developed flow-through nematode filter (FTNF). This developed biochip provides a new diagnostic method for parasitic detection from native blood samples. Pressure and velocity profiles have been calculated to predict the pressure drop to secure the efficiency of the developed device. A range of microcapillary structures within different microfluidic devices have been designed, fabricated and tested to uncover dirofilarioses from blood samples. Our results show that this passive filtration device can be used to speed up current diagnostic processes. A parasite detection platform has been constructed to automate the procedure decreasing diagnostic costs and time. The obtained structure is able to use for detection of other specific parasites. Due to the applied materials, the FTNF device also can be loaded by the degas-driven flow avoiding the usage of external syringe pumps to create a laboratory-independent construction. Finally, the developed FTNF biochip could be useful to monitor the presence of nematode during the time course of a treatment targeting nematodes and analyse the efficiency of the treatment.

Chapter 4

Deterministic Lateral Displacement Based Fractionation

4.1 Separation of Microvesicle from Serological Samples

As it was discussed in Chapter 2, the blood can be considered as a diagnostic tool for monitoring the body condition of the patient. The blood contains inestimable information reaching that from the condition of the cells but also the composition of plasma. The extracellular space of multicellular organisms contains solutions of metabolites, ions, proteins and polysaccharides and a large number of mobile membrane-bounded vesicles, called extracellular vesicles such as exosomes (Exs), microvesicles (MVs) and apoptotic bodies (ABs) [162]. The size ranges of major blood components is represented in Fig. 4.1.

Recent advances in the study of tumor-derived microvesicles reveal new insights into the cellular basis of disease progression and the potential to translate this knowledge into innovative approaches for cancer diagnostics and personalized therapy [163]. A key step in cancer diagnostics and molecular biological observations is to separate cells, functionalized microbeads, extracellular vesicles, or other particles from a solution which may contain other undesirable elements [30]. Even though a number of microfluidic techniques have been developed to enhance on-chip blood fractionation [11], classification of membrane vesicles, protocols of their isolation and detection, molecu-

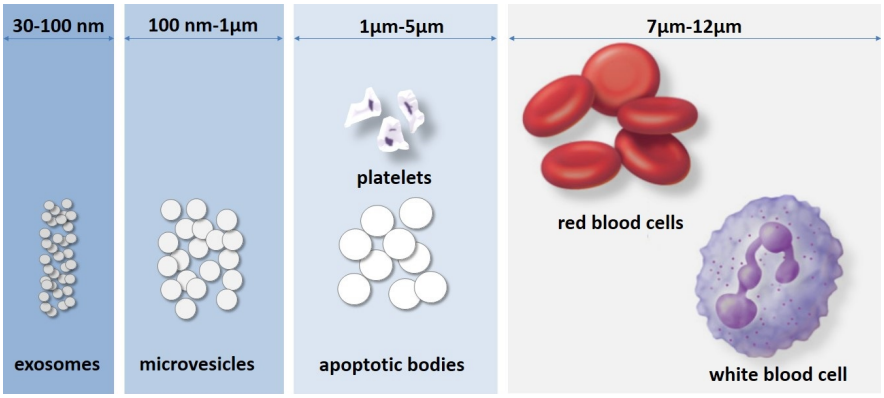

Figure 4.1: Size ranges of major blood components. While exosomes share size distribution with viruses, microvesicles overlap in size with bacteria and protein aggregates (e.g. immune complexes), apoptotic bodies and thrombocytes fall into the size range of $1-5\ \mu m$, the diameter of red blood cells is around $6-8\ \mu m$ and the size of lymphocytes is from $7\ \mu m$ up to $12\ \mu m$.

lar details of vesicular release, clearance and biological functions are still under intense investigation. The most frequently used methods to purify microvesicles and exosomes from cell culture supernatants or body fluids involve a series of centrifugation and filtration steps to remove cells, apoptotic bodies and other cellular contaminants by a final high-speed ultracentrifugation to pellet small extracellular vesicles [164]. These procedures require long preparation time, ultracentrifuge equipment and yield a relatively low amount of extracellular vesicles [165], making it difficult for application in clinical practice.

Due to the importance of the isolation of extracellular vesicles, several microfluidic devices have been developed for such purpose but these techniques mostly work in batch separation mode [166]. In the developed device, a continuous and label-free separation of microvesicles across functional laminar streamlines in pressure-driven microfluidic flow has been implemented using an asymmetric micropost array. By flowing serological samples through the functional streamlines, different-sized components can be fractionated for further biomedical diagnostic processes using the developed device.

A continuous-flow, label-free separation procedure reported by Huang et al. [88], known as deterministic lateral displacement (DLD), and shown in Fig. 4.2 is able to separate micrometer-sized particles enhancing on-chip blood fractionation with an uncertainty of 10 nm. The DLD technique is a size-based particle fractionation proce-

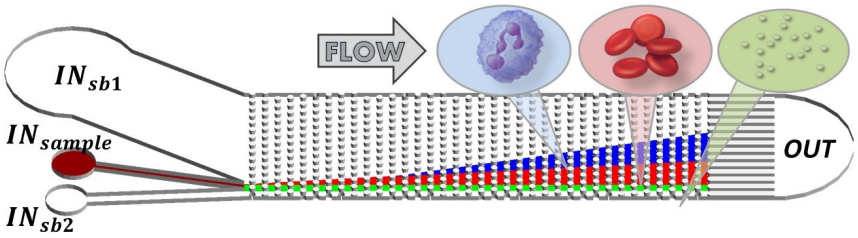

Figure 4.2: Overview image from the deterministic lateral displacement device. The serological sample (IN_{sample}) is focused by the lateral shear buffer solutions (IN_{SB1} and IN_{SB1}). The different-sized particles are fractionated along the column structure (leukocytes (blue), erythrocytes (red), and microvesicles (green)).

Application	Critical diameter (D_c)	Post shape	References
Leukocytes	From 3 μm to 23 μm	Circular	[86, 91, 96, 167]
Erythrocytes	From 3 μm to 9 μm	Circular, square, I-shape	[168, 169]
Thrombocytes	From 2.3 μm to 5.3 μm	Circular	[97]
Plasma	From 1 μm to 4 μm	Circular	[91]
Circulating tumor cells	From 5 μm to 7 μm	Circular, triangular	[84, 100, 170]
Nematodes, infections, pathogens	From 1.2 μm to 15 μm	Circular, I-shape	[83, 88, 90, 92, 95, 98, 168]

Table 4.1: Serological applications of the deterministic lateral displacement [171]. The critical diameter (D_c) determines the size of separated particles.

dure which has shown extremely high size selectivity, adaptability to sorting multiple particle sizes, and a broad range of operating conditions, sorting particles from submicrometer scale up to millimeter scale [87–89, 91, 92, 101, 172–178] with even a resolution of down to 10 nm [88]. This technique which shows a marked improvement over existing methods [171], has been shown capable of separating erythrocytes (RBCs), white blood cells (WBCs), thrombocytes, plasma, circulating tumor cells and nematodes/infections/pathogens from whole blood based on their size and summed into Table 4.1. Being a continuous separation method, DLD has all the advantages that such methods have to offer.

4.2 Device Design and Fabrication

Channel layouts were designed using AutoCAD 2013 (Autodesk Inc., San Rafael, CA, USA) and devices were produced using standard microfabrication soft-lithographic techniques [161,179] by casting polydimethylsiloxane (PDMS, Sylgard 184, Dow Corning, USA) on a SU-8 (MicroChem, Newton, MA, USA) positive relief patterned mold on a 4" silicon wafer produced by photolithography. PDMS monomer and curing agent were mixed to a ratio of $10:1$ (v/v), degassed and poured over the master and set aside at $70°C$ for 2 h for crosslinking. The liquid PDMS pre-polymer conforms to the shape of the master and replicates the features of the master. The crosslinked PDMS was removed from the mold and 0.75 mm inlet and outlet ports were fabricated through the PDMS slab using a Harris Uni-Core biopsy punch (Ted Pella). The patterned PDMS slab was bonded to microscope glass slide following surface treatment by Plasma-preen II 863 (Plasmatic Systems Inc. North Brunswick, NJ, USA). Finally, Teflon tubes were inserted into the access holes for fluidic contacts. The depth of all channels used was 20 μm. As it was mentioned previously , the deterministic lateral displacement cascade consists of 15 different regions with different gap sizes. Figure 4.2) provides a schematic image of the layout of our microfluidic device, which shows how the biological sample enters on center inlet (IN_{sample}) and hydrodynamically focused by shield buffers (IN_{sb1}, IN_{sb2}) and pushed through the array structure. The 7560 μm-long DLD array terminates in an observation section in which the laterally displaced distance and the occurred dispersion could be measured optically in the termination set of parallel channels. These channels facilitate counting and binning of the cells for the histograms.

4.3 Sample Preparation

The **isolation of red bood cells (RBCs)** and **white blood cell (WBCs)** was based on Ficoll - Paque^{TM} process. Venous human blood was collected from a male healthy adult volunteer and diluted by buffer solution (PBS with 2 mM EDTA) at ratio of 1:1 (v/v). 35 mL of diluted blood was carefully layered over 15 mL of Ficoll-Paque (Ficoll-Paque PLUS, GE Healthcare Europe GmbH, Freiburg, Germany) in a 50 mL conical tube. The sample was centrifuged at 400 g for 20 $minutes$ at $20°C$ in a swinging-bucket rotor without brake. The isolated mononuclear cell layer (lymphocytes and monocytes) was carefully aspirated and transferred to a new conical tube. The conical

tube was filled by buffer (PBS with 2 mM EDTA), and the cells were resuspended and centrifuged at 300 g for 7 *minutes* at 20°C. The supernatant was removed and the cell pellet, which contained WBCs, was resuspended in basic media (RPMI-1640 with 10% FBS) (sample A). RBCs were harvested from the first 50 mL conical tube from the pellet, and resuspended in basic media (RPMI-1640 with 10% FBS) (sample B).

For **isolation of microvesicles** we used a purification procedure as described previously by Turiák, Misják et al. [180]. The first steps are designed to eliminate cells and large extracellular vesicles by successive centrifugations at increasing speeds at each of these steps, the pellet was discarded and the supernatant was used for the following step. Firstly, the conditioned medium, which mainly contains microvesicles (MVs) and exosomes (Exs) but also contained some apoptotic bodies (ABs) from BV-2 cell culture (mouse, C57BL/6, brain, microglial cells), was centrifuged at 300 g for 20 minutes at 17°C. The pellet consisting of cells was discarded and the supernatant was transferred to conical tubes. Next, apoptotic bodies were removed from the supernatant by centrifuging it at 2000 g for 20 minutes at 17°C. The supernatant was submitted for further centrifugation. Finally the supernatant (enriched in microvesicles and exosomes) was centrifuged at 20000 g for 40 minutes at 4°C, and the microvesicle pellet was resuspended in 0.5 ml PBS. This microvesicle preparation was added to cell- and platelet-depleted blood plasma (sample C).

4.4 Experimental Setup

Pressure-driven flow was created using syringe pumps (NE-4000, New Era Pumping System Inc, Farmingdale, NY, USA) attached to the inlet via Teflon tubes, which made it possible to hydrodynamically focus the sample into a stream of 20 μm in width. Typical flow rates were used between 0.01 ml/h and 0.1 ml/h, controlled by the syringe pump. Imaging was performed on an inverted Olympus IX71 microscope (Olympus, Tokyo, Japan). Image recording was through a EyeRIS camera system (Eye-RIS Vision System-on-Chip, Anafocus, Spain).

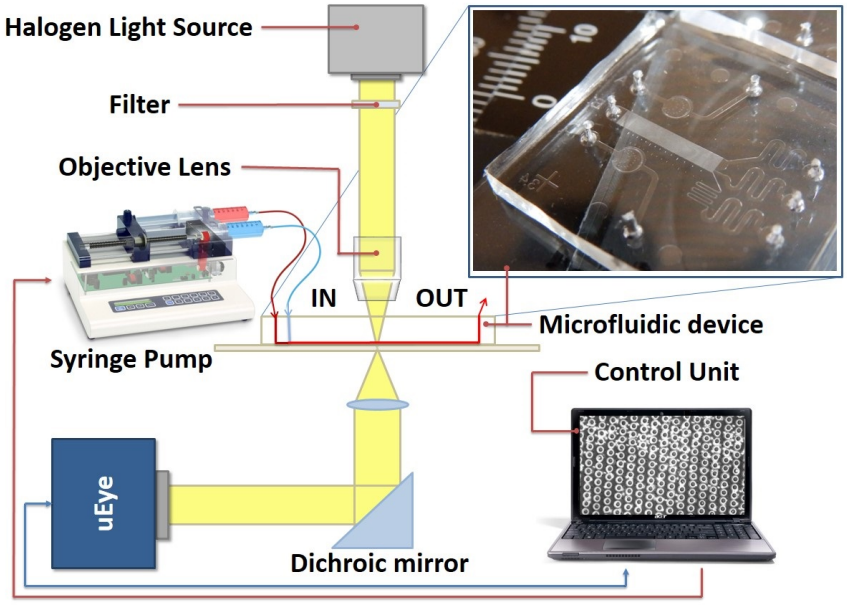

Figure 4.3: Schematic view of our experimental setup. The platform consists of computer-controlled syringe pump system, a microfluidic device on an inverted microscope, and USB color CCD camera.

4.5 Experimental Results

Extracellular vesicles provide a means for cells to interact with each other and appear to play an important role in cancer research and in a wide variety of physiological and pathological processes. In this study, on-chip microvesicle fractionation from biologically complex samples, such as human blood and conditioned medium from cultured cells was achieved for the first time using a deterministic lateral displacement array structure. Compared to the current standard protocols for isolating microvesicles, our deterministic lateral displacement device is faster, cheaper, label-free and its efficiency is comparable with clinical laboratory procedures.

A composition of the purified blood components (sample D = sample A + sample B + sample C, w/w 1:1:1), such as RBCs, WBCs and microvesicles, were loaded into the center inlet (IN_{Sample}) whereas the sheathed buffer (PBS) was introduced at the from ports on the left (IN_{sb1}) and right (IN_{sb2}) sides of the specimen port focusing samples to the desired width (Fig. 4.2). The concentration of RBCs (sample A) was around $5 \cdot 10^6$ per μL, WBCs (sample B) were around $7 \cdot 10^3$ per μL and microvesicles (sample C) were

around $8 \cdot 10^4$ per μL. Thrombocytes and apoptotic bodies have been extracted from the sample helping further optical classifications. During the measurements negligible population of the WBCs has been attached to the surface of the obstacles thus the purity and the loesses of applied process could be conserved.

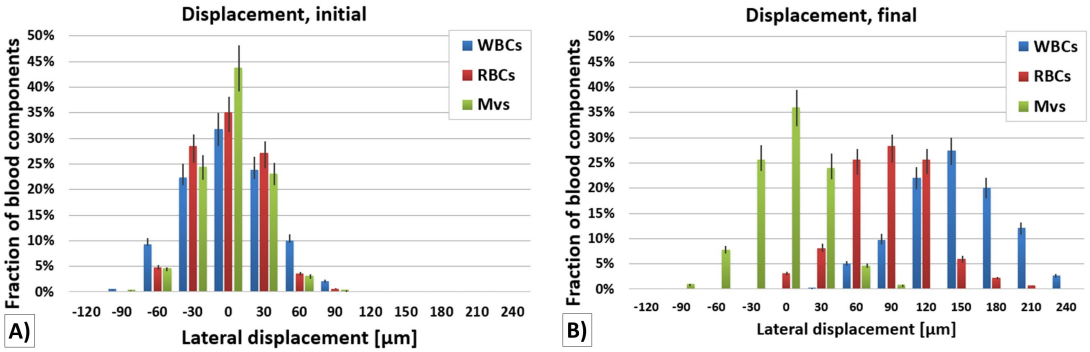

Figure 4.4: The efficiency of the cell separation using our developed DLD device (white blood cells (WBCs, blue), red blood cells (RBCs, red), and microvesicles (MVs, green)). A) The dispersion of the cell components in the initial section ($n = 1$). B) The lateral displacement of the cell components in the final section ($n = 15$). The error bar displays the standard deviations.

To optically detect the blood elements, the biological sample (sample D) is driven through the device at 0.001 ml/h flow rate which provides a suitable rate of cells for counting and a suitable residence time in front of the camera to be imaged. We record the lateral position of particles from the center of the inlet at two different positions along the device ($n = 1$ and $n = 15$) in the DLD array and bin the results of 10 different measurements into histograms which are shown in Fig. 4.4. Around $1.47 \cdot 10^5$ of particles has been optically distinguished and classified into WBCs, RBCs and microvesicles by an own developed algorithm.

The microvesicles, which are below any critical hydrodynamic diameter $D_{c,n}$, are able to follow a given stream through the array in zigzagging mode whereas RBCs and WBCs become laterally displaced by every interaction with posts. The further displacement of WBCs comes, when the diameter of RBCs becomes equal with the actual critical diameterand RBCs enter in zigzagging mode meanwhile WBCs are forced to adopt orientations that give them a greater displacement along the device.

Shear forces, which result from gradients in the fluid velocity around a particle may

induce complex motions including rotation, tumbling and shape change [169]. RBCs and WBCs can be considered as deformable and non-spherical particles, which suggests that such blood cells appear to modify their shape and diameter as they pass through the DLD device which can lead to lower separation efficiency. The behavior of blood components in the developed DLD array results in smooth histograms (Fig. 4.4). The displacement of RBCs, WBCs and microvesicles are observed at the terminal section by CCD camera-based image recording system.

The overview of our DLD structure is shown in Fig. **??**. The displacement of the different particles are bin for the histograms at the initial section (Fig. 4.4.A)and the end of our DLD array (Fig. 4.4.B). The position of microvesiclesremains mainly at the initial along the device due to the dimensionless numbers of fluid dynamics (Re_p<1, Pe>1 and St<1). The lateral displacement of RBCs from the center of the inlet is around $100-120\ \mu m$ from the initial and to the terminal section. Although the WBCs are displaced by $140-160\ \mu m$ from the initial position. The obtained and reported efficiency of fractionation can be increased by a longer device and the throughput by parallelized microfluidic devices.

4.6 Image processing algorithm for cell counting applications

A CNN-based algorithm has been developed, which is able to count particles in continuous liquid flow using these image processing steps. The used EyeRIS camera contains a Qeye SIS (Smart Image Sensor) and FPP (Focal Plane Processor) system. These Qeye SIS includes signal processors with local connections. On the other hand, the main advantages of the FPP system are the image recording and the image processing capabilities in the same architectural unit in real-time. The flow analyzer algorithm is executed on a 144x176 pixel resolution processor network and each pixel can be considered as a CNN cell unit. The image processing functions are supported by 7 Local Analogical Memories (LAM) and 4 Local Digital Memories (LDM). The fist type of memory can store the image in greyscale, while the digital one as a binary image. The image recording time of the binary images can be as high as 10000 frames per second. The camera is able to record in HDR (High Dynamic Range) also in 80 dB scale. The EyeRIS camera contains not only the sensor system, but also other hardware. The

NIOS II processor is the most important element after the sensor network, which is based on FPGA technology. This component makes the connection with the PC, and communicates with the other devices. The camera also contains serial flash memory. To help and accelerate the digital image processing functions a DICop (Digital Image CoProcessor) is also integrated, which is able to execute geometric transformations and PtP (Pixel-to-Pixel) transformations. A cell counting algorithm also has been developed on a fast-camera system (Eye-RIS Vision System) for cell counting applications in the observation outlets of the DLD device. The image processing is a commonly used method to analyze and record movements. The main difficulty of these processes is the object-background segmentation, which are not simple methods to discriminate. In general, the static object detection is insufficient because of the high variance of the background.

First of all, the recorded image contains noises form the sensor and external cases. The elimination of these errors need correction, especially if the diameter of the objects are just few pixels. After the image filtration, which can help to eliminate this problem, the main goal is to determine the shape of objectives from the background. The developed algorithm is the next: image recognition, Gaussian filter, global threshold, morphologic erosion, morphologic dilatation, morphologic centering, and cell/object counting. The proposed algorithm works with grey-scale and binary images and contains four main parts. First of all, it starts with the image recognition, continues the preprocessing part with filtration. Thirdly, the algorithm performs the binary image processing steps, which start with the threshold measurements, and terminate with one pixel in the middle of recognized cells. Finally, the cells/particles are counted from the result images.

4.6.1 Image recognition

This algorithm sequence performs the optical image acquisition that represents in the field of view of the Eye-RIS Vision System. During the measurement the integration time (also called exposure time) is highly correlated to the light intensity ($expTime = 0.7\ ms$). The observation output channels of the DLD structure is monitored (*SensedImg N*, showed in Fig. 4.5.A). The camera has a limited $144x176$ resolution, the work field is around 190 μm x 230 μm and the RBCs are around 5-6 pixels.

4.6.2 Preprocessing

The sensed image (*SensedImg N*, Fig. 4.5.A) could be infected with different noises by the sensor or external causes. The proposed algorithm starts with a Gaussian filter to reduce the one pixel noise (*GaussianImg N*, Fig. 4.5.B). In our case, this preprocessing function implements a low-pass filter that emulates a Gaussian filter using the resistive grid module available in the SIS Q-Eye. The resistive grid module is extremely efficient in both speed and power consumption. The spatial bandwidth of the filter is specified as the sigma parameter of the equivalent Gaussian filter ($sigmaValue = 0.4$).

4.6.3 Image processing algorithm

The conversion from gray-scale (*GaussianImg N*) to binary image (*ThreshImg N*, Fig. 4.5.C) is made by the global threshold value (GTV). The histogram of the gray-scale image is not flattened, the values of the pixels are between 100 and 145, but anyway we can consider a stable microfluidic system with fixed illumination ($TresholdValue = 115$). During this step the algorithm uses only one function, thus it is optimal in time, but not in quality. The fluctuation of the light can cause significant errors, if the noise size exceeds 2-3 pixels.

The erosion function on a binary image (*ErosionImg N*, Fig. 4.5.D) eliminates or reduces the noise. Before this step the image is inverted because the following functions work with white objects on black background. Two main methods exist for image erosion. The first is to use a predefined constant that allows to select between 4-neighbor connection and 8-neighbor connection or use a 3x3 pattern that completely defines the structuring element. Our algorithm is based on the first method with the 4-neighbor connection case and erases 1 pixels to open morphologically the objects and eliminate the one pixel errors.

The erosion function erases not only the noise and mistakes, but also consumes pixels from the objects, which is compensated by the algorithm in the next step. The dilatation is complementary to the morphological closing, it dilates a binary image in which objects are white and the background is black. After the dilatation function the cells have the same diameter on the result image (*DilatationImg N*, Fig. 4.5.E) like before the erosion. The second importance of dilatation is colligated to the next function.

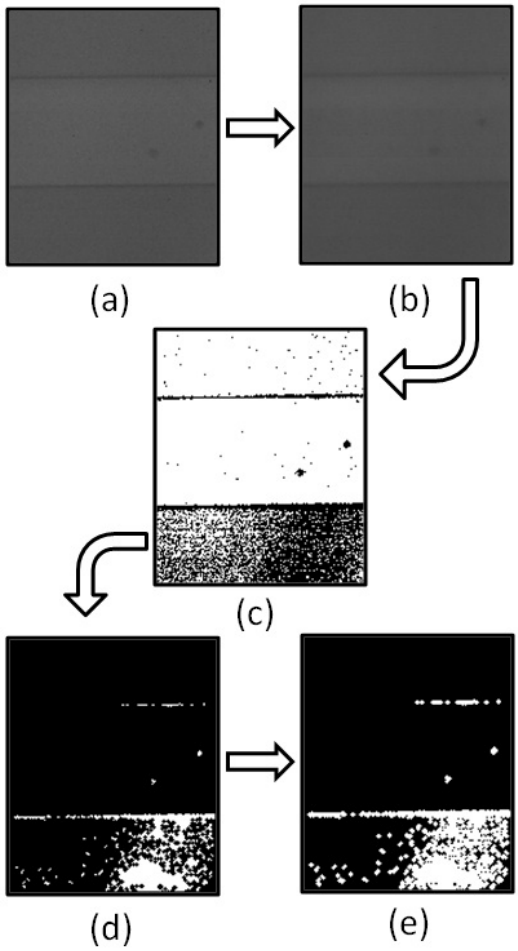

Figure 4.5: Cell detection algorithm. A) Grey-scale sensed image from the cell flow (*SensedImg N*). B) Gaussian filtering on the *SensedImg N* (*GaussianImg N*). C) Binary image is the result of use of threshold (*ThreshImg N*). D) The erosion function eliminates the noise from the image (*ErosionImg N*). E) Dilatation fills the holes on the cells (*DilatationImg N*).

The last step of the image precessing is the centering. This function gets the centroid positions of the objects (*CentroidImg N*). The morphological centroid peels the image one pixel off as many times as indicated in an input parameter. In our case, it iterates until no change occurs between iterations.

4.6.4 Counting Particles

The termination part of the algorithm counts the cells/particles inside the Region-Of-Interest (ROI), which is determined by a predefined binary mask (*MaskImg*). The result image (*ResultImg N*) is generated from a logical AND function of the *CentroidImg N* and the *MaskImg*. The number of the white pixels in the *ResultImg N* Images describes the number of the cells in the focused liquid flow. The efficiency of this algorithm was more than 90 percent.

4.7 Conclusion and outlook

Based on these experiments, the DLD array could be considered as a powerful tool for particle separation and manipulation. We could show the evidence that label-free fractionation of micron-scale particles can be delivered by using a deterministic lateral displacement array. This suggests that our DLD device may be able to provide rapid diagnostic information about the haemostatic condition of a blood sample, to explore cell-to-cell communication or to fractionate blood sample efficiently for clinical tests without the use of an activation specific label or marker. This chapter begins with a brave discussion about label-free separation techniques and the exact biomedical case has been introduced, which we worked on. We identified that the mechanism of separation is based on an inertial-based motion behaviour of the particles along the DLD structure. This causes that the inertial-based separation of particles, which was characterized by computational fluid dynamics simulation, shows correlations with our experimental measurements and results. Based on the theoretical works, we could develop an own designed DLD structure, which was useful to solve the initial challenge.

The main objective of this chapter was to produce cell-free plasma contacting extracellular vesicles from serological samples, which was archived successfully. In this version of developed device, we would like to understand better experimentally the functionality of the DLD structure, determine the position of outlets to raise the efficiency of separation; thus we designed this biochip with an observation part, which torrents into just one outlet. The cost of these aims was that we have no choice for any analysis of the output products, but only optically using an inverse light-microscopy. The efficiency of separation could be raised more by correcting the errors made in the design, that resulted in the dispersion of the particles and the clogging of the inertial

section during a long-term measurement. The main design errors were failing to account for providing inlets with a lower flow resistivity than the DLD column structure, designing inlets without pre-filters, the unequal-length of each section, and keeping the flow throughput without any interest. These errors could solved easily in the further design rising the efficiency of the separation significantly.

As it was mentioned ahead, the DLD can be used as a diagnostic tool for disease severity, assess the efficacy of different treatment strategies and possibly determine the eventual location of metastatic invasions for possible treatment. The DLD structure could be designed for sever purposes as biomedical sample preparation, chemical analysis or other industrial applications.

In biomedical sense, the DLD array system could be a useful analytic tool for further haemorheology. The human erythrocyte adopts a distinctive biconcave disc form in vivo. Any change or variety of theirs structure could highlight uncovered diseases as sicklemia, infection of malaria, or other blood-borne pathogens.

Another important field of application is the uncovering of circulating tumor cells (CTCs) and circulating clusters of cancer and stromal cells, which could be identified in the blood of patients by the presence of malignant cancer. CTCs constitute seeds for subsequent growth of additional tumors (metastasis) in vital distant organs, triggering a mechanism that is responsible for the vast majority of cancer-related deaths. The continuous observation or filtration of CTCs using DLD-based biochips could give us invaluable information.

Water is essential to life, but many people do not have access to clean and safe drinking water and many die of waterborne bacterial infections thus nowadays other challenging field, where the DLD structure could apply, is the observation of water-born pathogens from drinking water. The most important bacterial diseases transmitted through watercholera, typhoid fever and bacillary dysenteryis presented. Using the DLD structure with high throughput could be useful also to detect these water-borne pathogens.

Finally, I would like to mentioned, changing the separation range close or under micron-range could also have a fundamental interest in biomedical detection field as the fractionation of different-sized extracellular vesicles.

References

[1] G. M. Whitesides, "The origins and the future of microfluidics," *Nature*, vol. 442, no. 7101, pp. 368–373, Jul. 2006. 1, 3

[2] S. Haeberle and R. Zengerle, "Microfluidic platforms for lab-on-a-chip applications," *Lab on a Chip*, vol. 7, no. 9, pp. 1094–1110, Aug. 2007. 1

[3] D. R. Reyes, D. Iossifidis, P.-A. Auroux, and A. Manz, "Micro total analysis systems. 1. introduction, theory, and technology," *Analytical Chemistry*, vol. 74, no. 12, pp. 2623–2636, Jun. 2002. 1

[4] P.-A. Auroux, D. Iossifidis, D. R. Reyes, and A. Manz, "Micro total analysis systems. 2. analytical standard operations and applications," *Analytical Chemistry*, vol. 74, no. 12, pp. 2637–2652, Jun. 2002. 1

[5] T. M. Squires and S. R. Quake, "Microfluidics: Fluid physics at the nanoliter scale," *Reviews of Modern Physics*, vol. 77, no. 3, pp. 977–1026, Oct. 2005. 1

[6] C. D. Chin, V. Linder, and S. K. Sia, "Lab-on-a-chip devices for global health: Past studies and future opportunities," *Lab on a Chip*, vol. 7, no. 1, pp. 41–57, Dec. 2006. 1

[7] S. F. Ibrahim and G. v. d. Engh, "Flow cytometry and cell sorting," in *Cell Separation*, ser. Advances in Biochemical Engineering/Biotechnology, A. Kumar, I. Y. Galaev, and B. Mattiasson, Eds. Springer Berlin Heidelberg, Jan. 2007, no. 106, pp. 19–39. 1

[8] M. B. Dainiak, A. Kumar, I. Y. Galaev, and B. Mattiasson, "Methods in cell separations," in *Cell Separation*, ser. Advances in Biochemical Engineering/Biotechnology, A. Kumar, I. Y. Galaev, and B. Mattiasson, Eds. Springer Berlin Heidelberg, Jan. 2007, no. 106, pp. 1–18. 1, 2

[9] X.-J. J. Li and Y. Zhou, *Microfluidic Devices for Biomedical Applications*. Elsevier, Oct. 2013. 1

[10] D. R. Gossett, W. M. Weaver, A. J. Mach, S. C. Hur, H. T. K. Tse, W. Lee, H. Amini, and D. D. Carlo, "Label-free cell separation and sorting in microfluidic systems," *Analytical and Bioanalytical Chemistry*, vol. 397, no. 8, pp. 3249–3267, Aug. 2010. 1, 2

[11] H. W. Hou, A. A. S. Bhagat, W. C. Lee, S. Huang, J. Han, and C. T. Lim, "Microfluidic devices for blood fractionation," *Micromachines*, vol. 2, no. 3, pp. 319–343, Jul. 2011. 2, 38

[12] T. Chianea, N. E. Assidjo, and P. J. P. Cardot, "Sedimentation field-flow-fractionation: emergence of a new cell separation methodology," *Talanta*, vol. 51, no. 5, pp. 835–847, Apr. 2000. 2

[13] H. Pertoft, "Fractionation of cells and subcellular particles with percoll," *Journal of Biochemical and Biophysical Methods*, vol. 44, no. 1-2, pp. 1–30, Jul. 2000. 2

[14] P. Cuatrecasas and C. B. Anfinsen, "Affinity chromatography," *Annual Review of Biochemistry*, vol. 40, no. 1, pp. 259–278, 1971. 2

[15] P. Cuatrecasas, M. Wilchek, and C. B. Anfinsen, "Selective enzyme purification by affinity chromatography." *Proceedings of the National Academy of Sciences of the United States of America*, vol. 61, no. 2, pp. 636–643, Oct. 1968. 2

[16] P. Cuatrecasas, "Protein purification by affinity chromatography derivation of agarose and polyacrylamide beads," *Journal of Biological Chemistry*, vol. 245, no. 12, pp. 3059–3065, Jun. 1970. 2

[17] W. A. Bonner, H. R. Hulett, R. G. Sweet, and L. A. Herzenberg, "Fluorescence activated cell sorting," *Review of Scientific Instruments*, vol. 43, no. 3, pp. 404–409, Mar. 1972. 2

[18] A. Y. Fu, C. Spence, A. Scherer, F. H. Arnold, and S. R. Quake, "A microfabricated fluorescence-activated cell sorter," *Nature Biotechnology*, vol. 17, no. 11, pp. 1109–1111, Nov. 1999. 2

[19] C. S. Owen and N. L. Sykes, "Magnetic labeling and cell sorting," *Journal of Immunological Methods*, vol. 73, no. 1, pp. 41–48, Oct. 1984. 2

[20] I. Safarik and M. Safarikova, "Use of magnetic techniques for the isolation of cells," *Journal of Chromatography B: Biomedical Sciences and Applications*, vol. 722, no. 1-2, pp. 33–53, Feb. 1999. 2

[21] D. Pappas and K. Wang, "Cellular separations: A review of new challenges in analytical chemistry," *Analytica Chimica Acta*, vol. 601, no. 1, pp. 26–35, Oct. 2007. 2

[22] B. Mosadegh, T. Bersano-Begey, J. Y. Park, M. A. Burns, and S. Takayama, "Next-generation integrated microfluidic circuits," *Lab on a Chip*, vol. 11, no. 17, pp. 2813–2818, Aug. 2011. 3

[23] H. Craighead, "Future lab-on-a-chip technologies for interrogating individual molecules," *Nature*, vol. 442, no. 7101, pp. 387–393, Jul. 2006. 3

[24] D. Mark, S. Haeberle, G. Roth, F. v. Stetten, and R. Zengerle, "Microfluidic lab-on-a-chip platforms: requirements, characteristics and applications," *Chemical Society Reviews*, vol. 39, no. 3, pp. 1153–1182, Feb. 2010. 3

[25] D. Erickson and D. Li, "Integrated microfluidic devices," *Analytica Chimica Acta*, vol. 507, no. 1, pp. 11–26, Apr. 2004. 3

[26] T. A. Franke and A. Wixforth, "Microfluidics for miniaturized laboratories on a chip," *ChemPhysChem*, vol. 9, no. 15, pp. 2140–2156, Oct. 2008. 3

[27] P. S. Dittrich and A. Manz, "Lab-on-a-chip: microfluidics in drug discovery," *Nature Reviews Drug Discovery*, vol. 5, no. 3, pp. 210–218, Mar. 2006. 3

[28] A. Manz, N. Graber, and H. M. Widmer, "Miniaturized total chemical analysis systems: A novel concept for chemical sensing," *Sensors and Actuators B: Chemical*, vol. 1, no. 1-6, pp. 244–248, Jan. 1990. 3

[29] A. Manz, J. C. Fettinger, E. Verpoorte, H. Ludi, H. M. Widmer, and D. J. Harrison, "Micromachining of monocrystalline silicon and glass for chemical analysis systems a look into next century's technology or just a fashionable craze?" *TrAC Trends in Analytical Chemistry*, vol. 10, no. 5, pp. 144–149, May 1991. 3

[30] N. Pamme, "Continuous flow separations in microfluidic devices," *Lab on a Chip*, vol. 7, no. 12, pp. 1644–1659, Nov. 2007. 3, 4, 38

[31] J. C. Giddings, "A new separation concept based on a coupling of concentration and flow nonuniformities," *Separation Science*, vol. 1, no. 1, pp. 123–125, 1966. 4

[32] J. Shi, S. Yazdi, S.-C. S. Lin, X. Ding, I.-K. Chiang, K. Sharp, and T. J. Huang, "Three-dimensional continuous particle focusing in a microfluidic channelvia standing surface acoustic waves (SSAW)," *Lab on a Chip*, vol. 11, no. 14, pp. 2319–2324, Jun. 2011. 5

[33] J. Shi, H. Huang, Z. Stratton, Y. Huang, and T. J. Huang, "Continuous particle separation in a microfluidic channel via standing surface acoustic waves (SSAW)," *Lab on a Chip*, vol. 9, no. 23, pp. 3354–3359, Dec. 2009. 5

[34] J. Nam, H. Lim, D. Kim, and S. Shin, "Separation of platelets from whole blood using standing surface acoustic waves in a microchannel," *Lab Chip*, vol. 11, no. 19, pp. 3361–3364, Sep. 2011. 5

[35] T. Laurell, F. Petersson, and A. Nilsson, "Chip integrated strategies for acoustic separation and manipulation of cells and particles," *Chem. Soc. Rev.*, vol. 36, no. 3, pp. 492–506, Feb. 2007. 5

[36] J. Shi, X. Mao, D. Ahmed, A. Colletti, and T. J. Huang, "Focusing microparticles in a microfluidic channel with standing surface acoustic waves (SSAW)," *Lab on a Chip*, vol. 8, no. 2, pp. 221–223, Jan. 2008. 5

[37] T. Franke, S. Braunmuller, L. Schmid, A. Wixforth, and D. A. Weitz, "Surface acoustic wave actuated cell sorting (SAWACS)," *Lab on a Chip*, vol. 10, no. 6, pp. 789–794, Mar. 2010. 5

[38] Y. Li, C. Dalton, H. J. Crabtree, G. Nilsson, and K. V. I. S. Kaler, "Continuous dielectrophoretic cell separation microfluidic device," *Lab on a Chip*, vol. 7, no. 2, pp. 239–248, Jan. 2007. 5

[39] A. Valero, T. Braschler, A. Rauch, N. Demierre, Y. Barral, and P. Renaud, "Tracking and synchronization of the yeast cell cycle using dielectrophoretic opacity," *Lab Chip*, vol. 11, no. 10, pp. 1754–1760, May 2011. 5

[40] M. J. Hilhorst, G. W. Somsen, and G. J. de Jong, "Capillary electrokinetic separation techniques for profiling of drugs and related products," *Electrophoresis*, vol. 22, no. 12, pp. 2542–2564, Jul. 2001. 5

[41] H.-H. Cui, J. Voldman, X.-F. He, and K.-M. Lim, "Separation of particles by pulsed dielectrophoresis," *Lab on a Chip*, vol. 9, no. 16, pp. 2306–2312, Aug. 2009. 5

[42] S.-I. Han, S.-M. Lee, Y.-D. Joo, and K.-H. Han, "Lateral dielectrophoretic microseparators to measure the size distribution of blood cells," *Lab on a Chip*, vol. 11, no. 22, pp. 3864–3872, Oct. 2011. 5

[43] M. D. Vahey and J. Voldman, "Emergent behavior in particle-laden microfluidic systems informs strategies for improving cell and particle separations," *Lab on a Chip*, vol. 11, no. 12, pp. 2071–2080, Jun. 2011. 5

[44] L. Wang, L. A. Flanagan, N. L. Jeon, E. Monuki, and A. P. Lee, "Dielectrophoresis switching with vertical sidewall electrodes for microfluidic flow cytometry," *Lab on a Chip*, vol. 7, no. 9, pp. 1114–1120, Aug. 2007. 5

[45] H.-S. Moon, K. Kwon, S.-I. Kim, H. Han, J. Sohn, S. Lee, and H.-I. Jung, "Continuous separation of breast cancer cells from blood samples using multi-orifice flow fractionation (MOFF) and dielectrophoresis (DEP)," *Lab on a Chip*, vol. 11, no. 6, pp. 1118–1125, Feb. 2011. 5

[46] H. Lee, J. Jung, S.-I. Han, and K.-H. Han, "High-speed RNA microextraction technology using magnetic oligo-dT beads and lateral magnetophoresis," *Lab on a Chip*, vol. 10, no. 20, pp. 2764–2770, Oct. 2010. 5

[47] F. Shen, H. Hwang, Y. K. Hahn, and J.-K. Park, "Label-free cell separation using a tunable magnetophoretic repulsion force," *Analytical Chemistry*, vol. 84, no. 7, pp. 3075–3081, Feb. 2012. 5

[48] T. Zhu, R. Cheng, S. A. Lee, E. Rajaraman, M. A. Eiteman, T. D. Querec, E. R. Unger, and L. Mao, "Continuous-flow ferrohydrodynamic sorting of particles and cells in microfluidic devices," *Microfluidics and Nanofluidics*, vol. 13, no. 4, pp. 645–654, Oct. 2012. 5

[49] A. I. Rodriguez-Villarreal, M. D. Tarn, L. A. Madden, J. B. Lutz, J. Greenman, J. Samitier, and N. Pamme, "Flow focussing of particles and cells based on their intrinsic properties using a simple diamagnetic repulsion setup," *Lab on a Chip*, vol. 11, no. 7, pp. 1240–1248, Apr. 2011. 5

[50] D. Robert, N. Pamme, H. Conjeaud, F. Gazeau, A. Iles, and C. Wilhelm, "Cell sorting by endocytotic capacity in a microfluidic magnetophoresis device," *Lab on a Chip*, vol. 11, no. 11, pp. 1902–1910, Jun. 2011. 5

[51] N. Pamme and C. Wilhelm, "Continuous sorting of magnetic cells via on-chip free-flow magnetophoresis," *Lab on a Chip*, vol. 6, no. 8, pp. 974–980, Jul. 2006. 5

[52] P. Bhardwaj, P. Bagdi, and A. K. Sen, "Microfluidic device based on a micro-hydrocyclone for particle-liquid separation," *Lab on a Chip*, vol. 11, no. 23, pp. 4012–4021, Nov. 2011. 5

[53] D. Huh, J. H. Bahng, Y. Ling, H.-H. Wei, O. D. Kripfgans, J. B. Fowlkes, J. B. Grotberg, and S. Takayama, "Gravity-driven microfluidic particle sorting device with hydrodynamic separation amplification," *Analytical Chemistry*, vol. 79, no. 4, pp. 1369–1376, Jan. 2007. 5

[54] R. Gorkin, J. Park, J. Siegrist, M. Amasia, B. S. Lee, J.-M. Park, J. Kim, H. Kim, M. Madou, and Y.-K. Cho, "Centrifugal microfluidics for biomedical applications," *Lab on a Chip*, vol. 10, no. 14, pp. 1758–1773, Jun. 2010. 5

[55] S. Haeberle, T. Brenner, R. Zengerle, and J. Ducree, "Centrifugal extraction of plasma from whole blood on a rotating disk," *Lab on a Chip*, vol. 6, no. 6, pp. 776–781, May 2006. 5

[56] H. Zhang, E. Tu, N. D. Hagen, C. A. Schnabel, M. J. Paliotti, W. S. Hoo, P. M. Nguyen, J. R. Kohrumel, W. F. Butler, M. Chachisvillis, and P. J. Marchand, "Time-of-flight optophoresis analysis of live whole cells in microfluidic channels," *Biomedical Microdevices*, vol. 6, no. 1, pp. 11–21, Mar. 2004. 5

[57] B. S. Zhao, Y.-M. Koo, and D. S. Chung, "Separations based on the mechanical forces of light," *Analytica Chimica Acta*, vol. 556, no. 1, pp. 97–103, Jan. 2006. 5

[58] T.-H. Wu, Y. Chen, S.-Y. Park, J. Hong, T. Teslaa, J. F. Zhong, D. D. Carlo, M. A. Teitell, and P.-Y. Chiou, "Pulsed laser triggered high speed microfluidic fluorescence activated cell sorter," *Lab on a Chip*, vol. 12, no. 7, pp. 1378–1383, Mar. 2012. 5

[59] M. Kersaudy-Kerhoas, D. M. Kavanagh, R. S. Dhariwal, C. J. Campbell, and M. P. Y. Desmulliez, "Validation of a blood plasma separation system by biomarker detection," *Lab on a Chip*, vol. 10, no. 12, pp. 1587–1595, Jun. 2010. 5

[60] O. Forouzan, J. M. Burns, J. L. Robichaux, W. L. Murfee, and S. S. Shevkoplyas, "Passive recruitment of circulating leukocytes into capillary sprouts from existing capillaries in a microfluidic system," *Lab on a chip*, vol. 11, no. 11, pp. 1924–1932, Jun. 2011. 5

[61] S. Sugaya, M. Yamada, and M. Seki, "Observation of nonspherical particle behaviors for continuous shape-based separation using hydrodynamic filtration," *Biomicrofluidics*, vol. 5, no. 2, p. 24103, 2011. 5

[62] J. Marchalot, Y. Fouillet, and J.-L. Achard, "Multi-step microfluidic system for blood plasma separation: architecture and separation efficiency," *Microfluidics and Nanofluidics*, pp. 1–14, Dec. 2013. 5

[63] M. Yamada and M. Seki, "Microfluidic particle sorter employing flow splitting and recombining," *Analytical Chemistry*, vol. 78, no. 4, pp. 1357–1362, Feb. 2006. 5

[64] M. Kersaudy-Kerhoas, R. Dhariwal, M. P. Y. Desmulliez, and L. Jouvet, "Hydrodynamic blood plasma separation in microfluidic channels," *Microfluidics and Nanofluidics*, vol. 8, no. 1, pp. 105–114, Jan. 2010. 5

[65] A. I. Rodriguez-Villarreal, M. Arundell, M. Carmona, and J. Samitier, "High flow rate microfluidic device for blood plasma separation using a range of temperatures," *Lab on a chip*, vol. 10, no. 2, pp. 211–219, Jan. 2010. 5

[66] E. Sollier, M. Cubizolles, Y. Fouillet, and J.-L. Achard, "Fast and continuous plasma extraction from whole human blood based on expanding cell-free layer devices," *Biomedical microdevices*, vol. 12, no. 3, pp. 485–497, Jun. 2010. 5

[67] S. Yang, A. Undar, and J. D. Zahn, "A microfluidic device for continuous, real time blood plasma separation," *Lab on a Chip*, vol. 6, no. 7, pp. 871–880, Jun. 2006. 5

[68] D. H. Yoon, J. B. Ha, Y. K. Bahk, T. Arakawa, S. Shoji, and J. S. Go, "Size-selective separation of micro beads by utilizing secondary flow in a curved rectangular microchannel," *Lab on a Chip*, vol. 9, no. 1, pp. 87–90, Jan. 2009. 5

[69] W. C. Lee, A. A. S. Bhagat, S. Huang, K. J. V. Vliet, J. Han, and C. T. Lim, "High-throughput cell cycle synchronization using inertial forces in spiral microchannels," *Lab on a Chip*, vol. 11, no. 7, pp. 1359–1367, Apr. 2011. 5

[70] I. D. Johnston, M. B. McDonnell, C. K. L. Tan, D. K. McCluskey, M. J. Davies, and M. C. Tracey, "Dean flow focusing and separation of small microspheres within a narrow size range," *Microfluidics and Nanofluidics*, pp. 1–10, Jan. 2014. 5

[71] A. Russom, A. K. Gupta, S. Nagrath, D. D. Carlo, J. F. Edd, and M. Toner, "Differential inertial focusing of particles in curved low-aspect-ratio microchannels," *New Journal of Physics*, vol. 11, no. 7, p. 075025, Jul. 2009. 5

[72] A. A. S. Bhagat, S. S. Kuntaegowdanahalli, and I. Papautsky, "Continuous particle separation in spiral microchannels using dean flows and differential migration," *Lab on a Chip*, vol. 8, no. 11, pp. 1906–1914, Nov. 2008. 5

[73] A. A. S. Bhagat and S. S. Kuntaegowdanahalli, "Inertial microfluidics for continuous particle filtration and extraction," *Microfluidics and Nanofluidics*, vol. 7, no. 2, pp. 217–226, Aug. 2009. 5

[74] D. D. Carlo, "Inertial microfluidics," *Lab on a Chip*, vol. 9, no. 21, pp. 3038–3046, Nov. 2009. 5

[75] S. S. Kuntaegowdanahalli, A. A. S. Bhagat, G. Kumar, and I. Papautsky, "Inertial microfluidics for continuous particle separation in spiral microchannels," *Lab on a Chip*, vol. 9, no. 20, pp. 2973–2980, Oct. 2009. 5

[76] D. D. Carlo, D. Irimia, R. G. Tompkins, and M. Toner, "Continuous inertial focusing, ordering, and separation of particles in microchannels," *Proceedings of the National Academy of Sciences*, vol. 104, no. 48, pp. 18 892–18 897, Nov. 2007. 5

[77] S. Choi and J.-K. Park, "Tuneable hydrophoretic separation using elastic deformation of poly(dimethylsiloxane)," *Lab on a Chip*, vol. 9, no. 13, pp. 1962–1965, Jul. 2009. 5

[78] S. Choi and J. K. Park, "Sheathless hydrophoretic particle focusing in a microchannel with exponentially increasing obstacle arrays," *Analytical Chemistry*, vol. 80, no. 8, pp. 3035–3039, Apr. 2008. 5

[79] S. Choi, T. Ku, S. Song, C. Choi, and J. K. Park, "Hydrophoretic high-throughput selection of platelets in physiological shear-stress range," *Lab on a Chip*, vol. 11, no. 3, pp. 413–418, Feb. 2011. 5

[80] S. Choi and J.-K. Park, "Continuous hydrophoretic separation and sizing of microparticles using slanted obstacles in a microchannel," *Lab on a Chip*, vol. 7, no. 7, pp. 890–897, Jun. 2007. 5

[81] S. Choi, J. M. Karp, and R. Karnik, "Cell sorting by deterministic cell rolling," *Lab on a Chip*, vol. 12, no. 8, pp. 1427–1430, Apr. 2012. 5

[82] S. Choi, O. Levy, M. B. Coelho, J. M. S. Cabral, J. M. Karp, and R. Karnik, "A cell rolling cytometer reveals the correlation between mesenchymal stem cell dynamic adhesion and differentiation state," *Lab on a Chip*, vol. 14, no. 1, pp. 161–166, Nov. 2013. 5

[83] S. H. Holm, J. P. Beech, M. P. Barrett, and J. O. Tegenfeldt, "Separation of parasites from human blood using deterministic lateral displacement," *Lab on a chip*, vol. 11, no. 7, pp. 1326–1332, Apr. 2011. 5, 40

[84] J. P. Gleghorn, E. D. Pratt, D. Denning, H. Liu, N. H. Bander, S. T. Tagawa, D. M. Nanus, P. A. Giannakakou, and B. J. Kirby, "Capture of circulating tumor cells from whole blood of prostate cancer patients using geometrically enhanced differential immunocapture (GEDI) and a prostate-specific antibody," *Lab on a Chip*, vol. 10, no. 1, pp. 27–29, Jan. 2010. 5, 40

[85] N. Srivastava, C. Din, A. Judson, N. C. MacDonald, and C. D. Meinhart, "A unified scaling model for flow through a lattice of microfabricated posts," *Lab on a Chip*, vol. 10, no. 9, pp. 1148–1152, May 2010. 5

[86] S. Zheng, R. Yung, Y.-C. Tai, and H. Kasdan, "Deterministic lateral displacement MEMS device for continuous blood cell separation," in *18th IEEE International Conference on Micro Electro Mechanical Systems, 2005. MEMS 2005*, Jan. 2005, pp. 851–854. 5, 40

[87] K. Loutherback, K. S. Chou, J. Newman, J. Puchalla, R. H. Austin, and J. C. Sturm, "Improved performance of deterministic lateral displacement arrays with triangular posts," *Microfluidics and Nanofluidics*, vol. 9, no. 6, pp. 1143–1149, Dec. 2010. 5, 40

[88] L. R. Huang, E. C. Cox, R. H. Austin, and J. C. Sturm, "Continuous particle separation through deterministic lateral displacement," *Science*, vol. 304, no. 5673, pp. 987–990, May 2004. 5, 39, 40

[89] K. J. Morton, K. Loutherback, D. W. Inglis, O. K. Tsui, J. C. Sturm, S. Y. Chou, and R. H. Austin, "Crossing microfluidic streamlines to lyse, label and wash cells," *Lab on a Chip*, vol. 8, no. 9, pp. 1448–1453, Aug. 2008. 5, 40

[90] H. N. Joensson, M. Uhlen, and H. A. Svahn, "Droplet size based separation by deterministic lateral displacement-separating droplets by cell-induced shrinking," *Lab on a Chip*, vol. 11, no. 7, pp. 1305–1310, Apr. 2011. 5, 40

[91] J. A. Davis, D. W. Inglis, K. J. Morton, D. A. Lawrence, L. R. Huang, S. Y. Chou, J. C. Sturm, and R. H. Austin, "Deterministic hydrodynamics: Taking blood apart," *Proceedings of the National Academy of Sciences*, vol. 103, no. 40, pp. 14 779–14 784, Oct. 2006. 5, 40

[92] D. W. Inglis, N. Herman, and G. Vesey, "Highly accurate deterministic lateral displacement device and its application to purification of fungal spores," *Biomicrofluidics*, vol. 4, no. 2, p. 024109, Jun. 2010. 5, 40

[93] B. R. Long, M. Heller, J. P. Beech, H. Linke, H. Bruus, and J. O. Tegenfeldt, "Multidirectional sorting modes in deterministic lateral displacement devices," *Physical Review E*, vol. 78, no. 4, p. 046304, Oct. 2008. 5

[94] M. Heller and H. Bruus, "A theoretical analysis of the resolution due to diffusion and size dispersion of particles in deterministic lateral displacement devices," *Journal of Micromechanics and Microengineering*, vol. 18, no. 7, p. 075030, Jul. 2008. 5

[95] J. V. Green, M. Radisic, and S. K. Murthy, "Deterministic lateral displacement as a means to enrich large cells for tissue engineering," *Analytical Chemistry*, vol. 81, no. 21, pp. 9178–9182, Nov. 2009. 5, 40

[96] N. Li, D. Kamei, and C.-M. Ho, "On-chip continuous blood cell subtype separation by deterministic lateral displacement," in *2nd IEEE International Conference on Nano/Micro Engineered and Molecular Systems, 2007. NEMS '07*, Jan. 2007, pp. 932–936. 5, 40

[97] D. W. Inglis, K. J. Morton, J. A. Davis, T. J. Zieziulewicz, D. A. Lawrence, R. H. Austin, and J. C. Sturm, "Microfluidic device for label-free measurement of platelet activation," *Lab on a Chip*, vol. 8, no. 6, pp. 925–931, May 2008. 5, 40

[98] M. Al-Fandi, M. Al-Rousan, M. A. K. Jaradat, and L. Al-Ebbini, "New design for the separation of microorganisms using microfluidic deterministic lateral displacement," *Robotics and Computer-Integrated Manufacturing*, vol. 27, no. 2, pp. 237–244, Apr. 2011. 5, 40

[99] T. Bowman, J. Frechette, and G. Drazer, "Force driven separation of drops by deterministic lateral displacement," *Lab on a Chip*, vol. 12, no. 16, pp. 2903–2908, Jul. 2012. 5

[100] Z. Liu, F. Huang, J. Du, W. Shu, H. Feng, X. Xu, and Y. Chen, "Rapid isolation of cancer cells using microfluidic deterministic lateral displacement structure," *Biomicrofluidics*, vol. 7, no. 1, p. 011801, Jan. 2013. 5, 40

[101] D. W. Inglis, J. A. Davis, R. H. Austin, and J. C. Sturm, "Critical particle size for fractionation by deterministic lateral displacement," *Lab on a Chip*, vol. 6, no. 5, pp. 655–658, May 2006. 5, 40

[102] Y. Koh, H. Kang, S. H. Lee, J.-K. Yang, J.-H. Kim, Y.-S. Lee, and Y.-K. Kim, "Nanoslit membrane-integrated fluidic chip for protein detection based on size-dependent particle trapping," *Lab on a Chip*, vol. 14, no. 1, pp. 237–243, Nov. 2013. 5

[103] P. Lv, Z. Tang, X. Liang, M. Guo, and R. P. S. Han, "Spatially gradated segregation and recovery of circulating tumor cells from peripheral blood of cancer patients," *Biomicrofluidics*, vol. 7, no. 3, p. 034109, May 2013. 5

[104] H. M. Ji, V. Samper, Y. Chen, C. K. Heng, T. M. Lim, and L. Yobas, "Silicon-based microfilters for whole blood cell separation," *Biomedical Microdevices*, vol. 10, no. 2, pp. 251–257, Apr. 2008. 5

[105] H. Wei, B.-h. Chueh, H. Wu, E. W. Hall, C.-w. Li, R. Schirhagl, J.-M. Lin, and R. N. Zare, "Particle sorting using a porous membrane in a microfluidic device," *Lab on a Chip*, vol. 11, no. 2, pp. 238–245, Jan. 2011. 5

[106] K. Aran, A. Fok, L. A. Sasso, N. Kamdar, Y. Guan, Q. Sun, A. Undar, and J. D. Zahn, "Microfiltration platform for continuous blood plasma protein extraction from whole blood during cardiac surgery," *Lab on a Chip*, vol. 11, no. 17, pp. 2858–2868, Aug. 2011. 5

[107] J. S. Kuo, Y. Zhao, P. G. Schiro, L. Ng, D. S. W. Lim, J. P. Shelby, and D. T. Chiu, "Deformability considerations in filtration of biological cells," *Lab on a Chip*, vol. 10, no. 7, pp. 837–842, Apr. 2010. 5

[108] J. S. Shim and C. H. Ahn, "An on-chip whole blood/plasma separator using hetero-packed beads at the inlet of a microchannel," *Lab on a Chip*, vol. 12, no. 5, pp. 863–866, Feb. 2012. 5

[109] M. Nakashima, M. Yamada, and M. Seki, "Pinched flow fractionation (PFF) for continuous particle separation in a microfluidic device," in *Micro Electro Mechanical Systems, 2004. 17th IEEE International Conference on. (MEMS)*, 2004, pp. 33–36. 5

[110] T. Morijiri, S. Sunahiro, M. Senaha, M. Yamada, and M. Seki, "Sedimentation pinched-flow fractionation for size- and density-based particle sorting in microchannels," *Microfluidics and Nanofluidics*, vol. 11, no. 1, pp. 105–110, Jul. 2011. 5

[111] A. L. Vig and A. Kristensen, "Separation enhancement in pinched flow fractionation," *Applied Physics Letters*, vol. 93, no. 20, p. 203507, Nov. 2008. 5

[112] A. Jain and J. D. Posner, "Particle dispersion and separation resolution of pinched flow fractionation," *Analytical Chemistry*, vol. 80, no. 5, pp. 1641–1648, Mar. 2008. 5

[113] A. V. Larsen, L. Poulsen, H. Birgens, M. Dufva, and A. Kristensen, "Pinched flow fractionation devices for detection of single nucleotide polymorphisms," *Lab on a Chip*, vol. 8, no. 5, pp. 818–821, Apr. 2008. 5

[114] J. S. Dudani, D. R. Gossett, H. T. K. Tse, and D. D. Carlo, "Pinched-flow hydrodynamic stretching of single-cells," *Lab on a Chip*, vol. 13, no. 18, pp. 3728–3734, Aug. 2013. 5

[115] M. Yamada, M. Nakashima, and M. Seki, "Pinched flow fractionation:? continuous size separation of particles utilizing a laminar flow profile in a pinched microchannel," *Analytical Chemistry*, vol. 76, no. 18, pp. 5465–5471, Sep. 2004. 5

[116] A. A. S. Bhagat, H. W. Hou, L. D. Li, C. T. Lim, and J. Han, "Pinched flow coupled shear-modulated inertial microfluidics for high-throughput rare blood cell separation," *Lab on a Chip*, vol. 11, no. 11, pp. 1870–1878, Jun. 2011. 5

[117] C. Cupelli, T. Borchardt, T. Steiner, N. Paust, R. Zengerle, and M. Santer, "Leukocyte enrichment based on a modified pinched flow fractionation approach," *Microfluidics and Nanofluidics*, vol. 14, no. 3-4, pp. 551–563, Mar. 2013. 5

[118] O. Shardt, S. K. Mitra, and J. J. Derksen, "Lattice boltzmann simulations of pinched flow fractionation," *Chemical Engineering Science*, vol. 75, pp. 106–119, Jun. 2012. 5

[119] H. Lim, J. Nam, and S. Shin, "Lateral migration of particles suspended in viscoelastic fluids in a microchannel flow," *Microfluidics and Nanofluidics*, pp. 1–10, Feb. 2014. 5

[120] A. Srivastav, T. Podgorski, and G. Coupier, "Efficiency of size-dependent particle separation by pinched flow fractionation," *Microfluidics and Nanofluidics*, vol. 13, no. 5, pp. 697–701, Nov. 2012. 5

[121] Y. Sai, M. Yamada, M. Yasuda, and M. Seki, "Continuous separation of particles using a microfluidic device equipped with flow rate control valves," *Journal of Chromatography A*, vol. 1127, no. 12, pp. 214–220, Sep. 2006. 5

[122] J. Takagi, M. Yamada, M. Yasuda, and M. Seki, "Continuous particle separation in a microchannel having asymmetrically arranged multiple branches," *Lab on a Chip*, vol. 5, no. 7, pp. 778–784, Jun. 2005. 5

[123] X. Zhang, J. M. Cooper, P. B. Monaghan, and S. J. Haswell, "Continuous flow separation of particles within an asymmetric microfluidic device," *Lab on a Chip*, vol. 6, no. 4, pp. 561–566, Mar. 2006. 5

[124] H. W. Hou, H. Y. Gan, A. A. S. Bhagat, L. D. Li, C. T. Lim, and J. Han, "A microfluidics approach towards high-throughput pathogen removal from blood using margination," *Biomicrofluidics*, vol. 6, no. 2, p. 024115, Jun. 2012. 5

[125] A. J. Laki, K. Ivan, E. Fok, and P. Civera, "Filtration of nematodes using an integrated microcapillary system," *BioNanoScience*, pp. 1–11, Oct. 2014. 6

[126] A. J. Laki, L. Botzheim, K. Ivn, V. Tamsi, and P. Civera, "Separation of microvesicles from serological samples using deterministic lateral displacement effect," *BioNanoScience*, pp. 1–7, Nov. 2014. 6

[127] J. E. Hall, *Guyton and Hall Textbook of Medical Physiology: Enhanced E-book*. Elsevier Health Sciences, Jul. 2010. 7, 8

[128] J. Mazumdar, *Biofluid Mechanics*. World Scientific, Nov. 1992. 8

[129] J. Szentágothai and M. Réthelyi, *Funkciális anatómia*. Medicina könyvkiadó RT., 2002. 9, 17

[130] J. Bec, H. Homann, and S. S. Ray, "Gravity-driven enhancement of heavy particle clustering in turbulent flow," *Physical Review Letters*, vol. 112, no. 18, p. 184501, May 2014. 13

[131] D. R. Lide, *CRC Handbook of Chemistry and Physics, 85th Edition.* CRC Press, Jun. 2004. 14

[132] T. Kenner, H. Leopold, and H. Hinghofer-Szalkay, "The continuous high-precision measurement of the density of flowing blood," *Pflugers Archiv*, vol. 370, no. 1, pp. 25–29, Jan. 1977. 14

[133] W. L. Chandler and G. Schmer, "Evaluation of a new dynamic viscometer for measuring the viscosity of whole blood and plasma." *Clinical Chemistry*, vol. 32, no. 3, pp. 505–507, Mar. 1986. 14

[134] T. T. Nguyen, R. Mongrain, J. Brunette, O. F. Bertrand, J.-C. Tardif, and Y. Biadillah, "A method for matching the refractive index and kinematic viscosity of a blood analog for flow visualization in hydraulic cardiovascular models," *Journal of Biomechanical Engineering*, vol. 126, no. 4, pp. 529–535, Sep. 2004. 14

[135] J. Wang, W. Huang, R. S. Bhullar, and P. Tong, "Modeling of surface-tension-driven flow of blood in capillary tubes," *Mechanics & chemistry of biosystems: MCB*, vol. 1, no. 2, pp. 161–167, Jun. 2004. 14

[136] H. Jasper and T. C, "Cerebral blood flow and pH in excessive cortical discharge induced by metrazol and electrical stimulation," *Journal of Neurophysiology*, vol. 4, pp. 333–347, 1941. 14

[137] G. D. Lowe, F. G. Fowkes, J. Dawes, P. T. Donnan, S. E. Lennie, and E. Housley, "Blood viscosity, fibrinogen, and activation of coagulation and leukocytes in peripheral arterial disease and the normal population in the edinburgh artery study," *Circulation*, vol. 87, no. 6, pp. 1915–1920, Jan. 1993. 14

[138] C. Bonadonna, G. G. J. Ernst, and R. S. J. Sparks, "Thickness variations and volume estimates of tephra fall deposits: the importance of particle reynolds number," *Journal of Volcanology and Geothermal Research*, vol. 81, no. 3-4, pp. 173–187, May 1998. 14

[139] D. M. Eckmann, S. Bowers, M. Stecker, and A. T. Cheung, "Hematocrit, volume expander, temperature, and shear rate effects on blood viscosity," *Anesthesia & Analgesia*, vol. 91, no. 3, pp. 539–545, Jan. 2000. 18

[140] R. Fahraus and T. Lindqvist, "The viscosity of the blood in narrow capillary tubes," *American Journal of Physiology – Legacy Content*, vol. 96, no. 3, pp. 562–568, Jan. 1931. 18

[141] L. S. Garcia and D. A. Bruckner, *Diagnostic medical parasitology.* Elsevier, 1988. 19, 20

[142] A. Muro, C. Genchi, M. Cordero, and F. Simon, "Human dirofilariasis in the european union," *Parasitology Today (Personal Ed.)*, vol. 15, no. 9, pp. 386–389, Sep. 1999. 20, 24

[143] S. Pampiglione and F. Rivasi, "Human dirofilariasis due to dirofilaria (nochtiella) repens: an update of world literature from 1995 to 2000," *Parassitologia*, vol. 42, no. 3-4, pp. 231–254, Dec. 2000. 20

[144] E. Joseph, A. Matthai, L. K. Abraham, and S. Thomas, "Subcutaneous human dirofilariasis," *Journal of Parasitic Diseases: Official Organ of the Indian Society for Parasitology*, vol. 35, no. 2, pp. 140–143, Oct. 2011. 20

[145] F. Simón, J. López-Belmonte, C. Marcos-Atxutegi, R. Morchón, and J. R. Martín-Pacho, "What is happening outside north america regarding human dirofilariasis?" *Veterinary parasitology*, vol. 133, no. 2-3, pp. 181–189, Oct. 2005. 20

[146] C. Genchi, L. Venco, and M. Genchi, "Guideline for the laboratory diagnosis of canine and feline dirofilaria infections," *Mappe Parassitologiche*, pp. 139–144, Feb. 2007. 20, 23, 24, 37

[147] T. C. Orihel and M. L. Eberhard, "Zoonotic filariasis," *Clinical Microbiology Reviews*, vol. 11, no. 2, pp. 366–381, Apr. 1998. 21

[148] K. W. Knauer, "Human dirofilariasis," *Clinical Techniques in Small Animal Practice*, vol. 13, no. 2, pp. 96–98, May 1998. 21

[149] M. T. Manfredi, A. d. Cerbo, and M. Genchi, "Biology of filarial worms parasitizing dogs and cats." *Mappe Parassitologiche*, vol. 8, pp. 39–45, 2007. 22, 25

[150] M. A. Peribanez, J. Lucientes, S. Arce, M. Morales, J. A. Castillo, and M. J. Gracia, "Histochemical differentiation of dirofilaria immitis, dirofilaria repens and acanthocheilonema dracunculoides microfilariae by staining with a commercial kit, leucognost-SP," *Veterinary Parasitology*, vol. 102, no. 1?2, pp. 173–175, Dec. 2001. 24

[151] G. Lawrence T., G. Rb, B. Eb, M.-G. M, P. Gj, D. Lm, R. Cr, and M. Jb, "Serologic pattern of canine heartworm (dirofilaria immitis) infection." *American journal of veterinary research*, vol. 45, no. 6, pp. 1178–1183, Jun. 1984. 24

[152] L. Roth, L. Brown, S. Brum, L. F. M. Nelson, D. Reczeck, and D. v. Schantz, "Comparison of three diagnostic tests for dirofilaria immitis in a low-incidence area," *Journal of Veterinary Diagnostic Investigation*, vol. 5, no. 4, pp. 647–648, Oct. 1993. 24

[153] B. Santamaria, M. Cordero, A. Muro, and F. Simon, "Evaluation of dirofilaria immitis excretory/secretory products for seroepidemiological studies on human dirofilariosis," *Parasite (Paris, France)*, vol. 2, no. 3, pp. 269–273, Sep. 1995. 24

[154] F. Simon, G. Prieto, A. Muro, G. Cancrini, M. Cordero, and C. Genchi, "Human humoral immune response to dirofilaria species," *Parassitologia*, vol. 39, no. 4, pp. 397–400, Dec. 1997. 24

[155] L. Perera, J. L. Perez-Arellano, M. Cordero, F. Simon, and A. Muro, "Utility of antibodies against a 22 kD molecule of dirofilaria immitis in the diagnosis of human pulmonary dirofilariasis," *Tropical medicine & international health: TM & IH*, vol. 3, no. 2, pp. 151–155, Feb. 1998. 24

[156] G. Prieto, F. Simon, C. Genchi, J. W. McCall, and L. Venco, "Utility of adult antigens of dirofilaria immitis for the early detection of dirofilariosis and for the evaluation of chemoprophylactic treatment in experimentally infected cats," *Veterinary Parasitology*, vol. 86, no. 1, pp. 5–13, Sep. 1999. 24

[157] G. Favia, A. Lanfrancotti, A. della Torre, G. Cancrini, and M. Coluzzi, "Polymerase chain reaction-identification of dirofilaria repens and dirofilaria immitis," *Parasitology*, vol. 113 (Pt 6), pp. 567–571, Dec. 24

[158] G. Favia, A. Lanfrancotti, A. della Torre, and G. Cancrini, "Advances in the identification of dirofilaria repens and dirofilaria immitis by a PCR-based approach," *Parassitologia*, vol. 39, no. 4, pp. 401–402, Dec. 1997. 24

[159] G. Cancrini, G. Prieto, G. Favia, S. Giannetto, R. Tringali, M. Pietrobelli, and F. Simon, "Serological assays on eight cases of human dirofilariasis identified by morphology and DNA diagnostics," *Annals of Tropical Medicine and Parasitology*, vol. 93, no. 2, pp. 147–152, Mar. 1999. 24

[160] J. H. Theis, "Public health aspects of dirofilariasis in the united states," *Veterinary parasitology*, vol. 133, no. 2-3, pp. 157–180, Oct. 2005. 21

[161] J. C. McDonald and G. M. Whitesides, "Poly(dimethylsiloxane) as a material for fabricating microfluidic devices," *Accounts of Chemical Research*, vol. 35, no. 7, pp. 491–499, Jul. 2002. 29, 30, 41

[162] B. György, T. G. Szabó, M. Pásztói, Z. Pál, P. Misják, B. Aradi, V. László, E. Pállinger, E. Pap, A. Kittel, G. Nagy, A. Falus, and E. I. Buzás, "Membrane vesicles, current state-of-the-art: emerging role of extracellular vesicles," *Cellular and molecular life sciences: CMLS*, vol. 68, no. 16, pp. 2667–2688, Aug. 2011. 38

[163] C. D'Souza-Schorey and J. W. Clancy, "Tumor-derived microvesicles: shedding light on novel microenvironment modulators and prospective cancer biomarkers," *Genes & Development*, vol. 26, no. 12, pp. 1287–1299, Jun. 2012. 38

[164] C. Thery, S. Amigorena, G. Raposo, and A. Clayton, "Isolation and characterization of exosomes from cell culture supernatants and biological fluids," in *Current Protocols in Cell Biology*, J. S. Bonifacino, M. Dasso, J. B. Harford, J. Lippincott-Schwartz, and K. M. Yamada, Eds. Hoboken, NJ, USA: John Wiley & Sons, Inc., Apr. 2006. 39

[165] H. G. Lamparski, A. Metha-Damani, J.-Y. Yao, S. Patel, D.-H. Hsu, C. Ruegg, and J.-B. Le Pecq, "Production and characterization of clinical grade exosomes derived from dendritic cells," *Journal of Immunological Methods*, vol. 270, no. 2, pp. 211–226, Dec. 2002. 39

[166] C. Chen, J. Skog, C.-H. Hsu, R. T. Lessard, L. Balaj, T. Wurdinger, B. S. Carter, X. O. Breakefield, M. Toner, and D. Irimia, "Microfluidic isolation and transcriptome analysis of serum microvesicles," *Lab on a Chip*, vol. 10, no. 4, pp. 505–511, Feb. 2010. 39

[167] D. W. Inglis, M. Lord, and R. E. Nordon, "Scaling deterministic lateral displacement arrays for high throughput and dilution-free enrichment of leukocytes," *Journal of Micromechanics and Microengineering*, vol. 21, no. 5, p. 054024, May 2011. 40

[168] K. K. Zeming, S. Ranjan, and Y. Zhang, "Rotational separation of non-spherical bioparticles using i-shaped pillar arrays in a microfluidic device," *Nature Communications*, vol. 4, p. 1625, Mar. 2013. 40

[169] J. P. Beech, S. H. Holm, K. Adolfsson, and J. O. Tegenfeldt, "Sorting cells by size, shape and deformability," *Lab on a chip*, vol. 12, no. 6, pp. 1048–1051, Mar. 2012. 40, 45

[170] K. Loutherback, J. D'Silva, L. Liu, A. Wu, R. H. Austin, and J. C. Sturm, "Deterministic separation of cancer cells from blood at 10 mL/min," *AIP Advances*, vol. 2, no. 4, Oct. 2012. 40

[171] J. McGrath, M. Jimenez, and H. Bridle, "Deterministic lateral displacement for particle separation: a review," *Lab on a Chip*, Sep. 2014. 40

[172] Y. S. Lubbersen, M. A. I. Schutyser, and R. M. Boom, "Suspension separation with deterministic ratchets at moderate reynolds numbers," *Chemical Engineering Science*, vol. 73, pp. 314–320, May 2012. 40

[173] J. P. Beech and J. O. Tegenfeldt, "Tuneable separation in elastomeric microfluidics devices," *Lab on a Chip*, vol. 8, no. 5, pp. 657–659, Apr. 2008. 40

[174] R. Devendra and G. Drazer, "Gravity driven deterministic lateral displacement for particle separation in microfluidic devices," *Analytical Chemistry*, vol. 84, no. 24, pp. 10 621–10 627, Dec. 2012. 40

[175] T. Kulrattanarak, R. G. M. v. d. Sman, C. G. P. H. Schron, and R. M. Boom, "Analysis of mixed motion in deterministic ratchets via experiment and particle simulation," *Microfluidics and Nanofluidics*, vol. 10, no. 4, pp. 843–853, Apr. 2011. 40

[176] J. P. Beech, P. Jnsson, and J. O. Tegenfeldt, "Tipping the balance of deterministic lateral displacement devices using dielectrophoresis," *Lab on a chip*, vol. 9, no. 18, pp. 2698–2706, Sep. 2009. 40

[177] K. Loutherback, J. Puchalla, R. H. Austin, and J. C. Sturm, "Deterministic microfluidic ratchet," *Physical Review Letters*, vol. 102, no. 4, p. 045301, Jan. 2009. 40

[178] D. J. Collins, T. Alan, and A. Neild, "Particle separation using virtual deterministic lateral displacement (vDLD)," *Lab on a Chip*, vol. 14, no. 9, pp. 1595–1603, Apr. 2014. 40

[179] D. C. Duffy, J. C. McDonald, O. J. A. Schueller, and G. M. Whitesides, "Rapid prototyping of microfluidic systems in poly(dimethylsiloxane)," *Analytical Chemistry*, vol. 70, no. 23, pp. 4974–4984, Dec. 1998. 41

[180] L. Turiák, P. Misják, T. G. Szabó, B. Aradi, K. Pálóczi, O. Ozohanics, L. Drahos, A. Kittel, A. Falus, E. I. Buzás, and K. Vákey, "Proteomic characterization of thymocyte-derived microvesicles and apoptotic bodies in BALB/c mice," *Journal of proteomics*, vol. 74, no. 10, pp. 2025–2033, Sep. 2011. 42